nature communications

Article

https://doi.org/10.1038/s41467-024-55170-5

Macrophage STING signaling promotes fibrosis in benign airway stenosis via an IL6-STAT3 pathway

Received: 17 May 2024

Accepted: 4 December 2024

Published online: 03 January 2025

Check for updates

YiLin Chen[1,5], ChengCheng Yang[1,5], YuShan Miao[1,5], DongChen Shi[1], Xiang Li[2], Sen Tian[3], YiFei Zhang[1], ChengFei Xu[1], YuChao Dong[1], ChaoFeng Han[4] ✉, Hui Shi[1] ✉ & Chong Bai[1] ✉

Acute and chronic inflammation are important pathologies of benign airway stenosis (BAS) fibrosis, which is a frequent complication of critically ill patients. cGAS-STING signalling has an important role in inflammation and fibrosis, yet the function of STING in BAS remains unclear. Here we demonstrate using scRNA sequencing that cGAS–STING signalling is involved in BAS, which is accompanied by increased dsDNA, expression and activation of STING. STING inhibition or deficiency effectively alleviates tracheal fibrosis of BAS mice by decreasing both acute and chronic inflammation. Macrophage depletion also effectively ameliorates BAS. Mechanistically, dsDNA from damaged epithelial cells activates the cGAS-STING pathway of macrophages and induces IL-6 to activate STAT3 and promote fibrosis. In summary, the present results suggest that cGAS-STING signalling induces acute inflammation and amplifies the chronic inflammation and tracheal fibrosis associated with benign airway stenosis, highlighting the mechanism and potential drug target of BAS.

Benign airway stenosis (BAS) is a prevalent respiratory condition, characterized by varying degrees of respiratory distress and it can lead to asphyxia and even mortality in severe cases. The acute inflammation and chronic inflammation are the critical pathology of benign airway stenosis (BAS) fibrosis. The primary aetiologies of BAS are mechanical injuries, including postintubation tracheal stenosis (PITS), post-tracheotomy tracheal stenosis (PTTS), and postsurgical tracheal stenosis[1]. With the frequent occurrence of public health events, such as the COVID-19 incident in recent years, tracheal intubation is an important tool for treating critical care patients with lung failure[2]. However, long-term endotracheal intubation will lead to an increased risk of BAS. Currently, clinical interventions for BAS primarily encompass comprehensive bronchoscopic therapies, such as stent implantation and balloon dilation[3,4]. While surgical procedures demonstrate considerable effectiveness, they can also result in secondary injury, which leads to excessive hyperproliferation of granulation tissue granulation tissue and tracheal restenosis. Thus, identifying new therapeutic targets during airway injury to prevent the formation of BAS is crucial. In cases of recurrent cicatricial hyperplasia, some medications (such as mitomycin C, paclitaxel, or pirfenidone) can be utilized to inhibit the fibrosis process, effectively suppressing the development and recurrence of scar tissue[5–7]. Furthermore, the reports have suggested that the administration of antibiotics, hormones, and other anti-inflammatory medications during the inflammatory phase can yield therapeutic benefits in the treatment of tracheal stenosis[8,9]. The excessive inflammatory response frequently

[1]Department of Respiratory and Critical Care Medicine, The First Affiliated Hospital of Naval Medical University, Shanghai, China. [2]Department of Respiratory and Critical Care Medicine, General Hospital of Central Theater Command of Chinese People's Liberation Army, Wuhan, China. [3]Department of Respiratory and Critical Care Medicine, No. 906 Hospital of the Chinese People's Liberation Army Joint Logistic Support Force, Ningbo, China. [4]Department of Histology and Embryology, Naval Medical University, Shanghai, China. [5]These authors contributed equally: YiLin Chen, ChengCheng Yang, YuShan Miao.
✉e-mail: hcf@immunol.org; Shihui@smmu.edu.cn; Chongbai@smmu.edu.cn

serves as a significant contributing factor to the development of airway stenosis, and timely inhibition of this response can effectively alleviate the severity of stenosis.

The cGAS-STING pathway serves as a crucial component of innate immunity, acting as a defence mechanism. DNA can stimulate immune responses, and when the cGAS-STING pathway detects abnormal DNA, such as from bacteria, DNA viruses, and self-DNA released from the nucleus, mitochondria, and dying cells, it becomes activated, leading to the generation of type I interferons (IFNs) and proinflammatory cytokines[10,11]. Several studies have revealed that the cGAS-STING pathway not only plays a protective role in combating foreign pathogens but also plays a significant role in the initiation and progression of various conditions such as infections, inflammation, tumors, autoimmune diseases, and other diseases[12]. Moreover, reports have revealed the involvement of the STING pathway in the pathogenesis of fibrotic diseases, including pulmonary fibrosis, liver fibrosis, and renal fibrosis[13–15]. STING is highly expressed on haematopoietic cells, such as macrophages[16],and the presence of macrophages is essential for the proper healing of wounds. When macrophages become dysregulated and excessive inflammatory factors are released, abnormal wound healing can occur, resulting in the formation of scar tissue[17]. Previous studies have demonstrated that dsDNA released after myocardial injury activates STING in macrophages, thereby promoting myocardial fibrosis in mice with myocardial infarction[18]. However, the relationship between macrophage STING signalling and BAS remains elusive.

In this work, we find that signalling through STING is involved in the development of BAS. The present study provides evidence that dsDNA released after tracheal injury activates the cGAS-STING pathway in mice with BAS, and that inhibition of STING alleviates fibrosis in benign airway stenosis. Mechanistically, the activation of STING in macrophages by dsDNA upon tracheal injury induces the inflammatory factor IL-6, which further activates fibroblasts via the IL-6-STAT3 axis and promotes fibrosis. Thus, the present findings suggest that the cGAS-STING pathway is a potential therapeutic target for preventing BAS.

Results

Single-cell RNA sequencing reveals the expression of the cGAS–STING pathway in granulation tissue from patients with BAS

Single-cell RNA sequencing (scRNA-seq) is widely used for the study of diseases, offering unparalleled insights into cellular heterogeneity. scRNA-seq were performed to examine the cellular identity and investigate the expression heterogeneity of the cGAS-STING pathway in BAS, which is closely associated with acute and chronic inflammation.

Three normal tracheal tissues (normal group) and four granulation tissues (granulation group) were collected for scRNA-seq. In total, 31,478 cells were captured in the normal group, and 27,108 cells were captured in the granulation group (Fig. 1a). The formation of distinct transcriptomic clusters in uniform manifold approximation and projection (UMAP) space was observed, with the clusters reflecting the cell type or group (Fig. 1b, c). The cells were divided into the following 14 clusters according to marker genes: B cells, basal cells, ciliated cells, endothelial cells, epithelial cells, fibroblasts, mast cells, macrophages, neutrophils, plasma cells, proliferating cells, SMCs, T cells, and Type II alveolar cells (Fig. 1d). These 14 clusters of cells were divided into three main groups, namely, epithelial cells, resident cells, and immune cells. The percentage of immune cells was significantly greater in the granulation group than in the normal group (Fig. 1e). GSEA analysis suggested that the most significantly enriched Go term was inflammatory response in Granulation group compare to Normal group (Fig. 1f). This is consistent with the pathological features of acute and chronic inflammation in BAS. In addition, enriched Go terms were also closely related to immune response (Fig. 1f). Further analysis revealed that Cytosolic DNA sensing pathway which closely related to immune response was highly enriched in granulation tissue (Fig. 1g). After analysis of the gene expression levels of *cGAS* and *STING* found that both *cGAS* and *STING* were expressed within most of clusters (Fig. 1h). It has been confirmed that STING and cGAS were commonly expressed in both immune and nonimmune cells[19,20]. In contrast to the general expression of *STING* and *cGAS* in most of cell clusters, the high scores for the cGAS-STING pathway were mainly concentrated in immune cells, including macrophages, T cells, and neutrophils (Fig. 1i). The cGAS-STING pathway score was greater in the granulation group than in the normal group (Fig. 1j). Next, the cGAS–STING pathway scores were assessed in each cluster of the granulation group, which revealed the highest score in the macrophage cluster (Fig. 1k). Taken together, the scRNA-seq data suggested that the cGAS–STING pathway, in which macrophages play an important role, is highly expressed in the granulation tissue of patients with benign airway stenosis.

cGAS-STING signalling is activated in BAS

The release of double-stranded DNA (dsDNA) from damaged or dead cells is a key event in the initiation of an inflammatory response. Benign airway stenosis is a pathological condition characterized by acute and chronic inflammation resulting from damage to the large central airways caused by tracheal intubation or the placement of a tracheal stent (Supplementary Fig. 1). Following bronchoscopic lavage in patients with benign airway stenosis, the dsDNA content of tracheal lavage fluid was significantly elevated in patients with benign airway stenosis compared with controls (Fig. 2a, b). To determine the role of the cGAS-STING pathway in BAS, a model of BAS was generated by using a brush to inflict damage on the trachea of mice (Fig. 2c). The histological results revealed that the mice in the control group had a patent trachea with an intact epithelium and no inflammatory cell infiltration or granulation tissue proliferation (Fig. 2d). In contrast, in the BAS group, the area of mechanical injury showed varying degrees of stenosis and significant granulomatous hyperplasia, with proliferation of tracheal epithelial cells, extensive inflammatory cell infiltration, excessive proliferation, disorganization of fibroblasts, and increased neovascularization, and excessive extracellular matrix deposition, resulting in thickening of the lamina propria (LP) (Fig. 2d). Notably, the LP thickness was greater in the BAS group than in the control group (Fig. 2e). Mouse tracheal tissues were collected at different time points for transcriptome sequencing. Gene Ontology (GO) analysis of the tracheal transcriptome revealed that the predominant manifestations included the inflammatory reaction elicited by the injury, immune system activation, and various biological processes associated with DNA in the initial 24 h period subsequent to tracheal scraping (Supplementary Fig. 2a). However, in the 7th day after modelling, the tracheal tissue was already in a state of repair, consisting mainly of regeneration of the tracheal ciliated epithelium, remodeling of the extracellular matrix and production of fibroblastic granulation tissue (Supplementary Fig. 2b), which suggested that the trachea of scraped mice underwent a physiological process consistent with sarcomere growth. Moreover, in the early stage of BAS, many molecular functions related to DNA are activated in the trachea of mice. Several studies have now demonstrated that DNA can activate the immune response[21]. Therefore, the present study evaluated the presence of double-stranded DNA (dsDNA) in control and injured tracheas, which revealed that that the dsDNA content in the tracheal lavage fluid in the BAS group was significantly greater than that in the control group (Fig. 2f). Moreover, IF analysis revealed that tracheal scraping led to prominent cytosolic dsDNA leakage in the trachea (Fig. 2g). Kyoto Encyclopaedia of Genes and Genomes (KEGG) pathway analysis of the upregulated differentially expressed genes (DEGs) revealed that the cytosolic DNA-sensing pathway was significantly activated in BAS at 24 h after tracheal injury (Fig. 2h). As shown by the heatmap of key DEGs, genes related to the cytosolic DNA-sensing pathway were highly expressed at 24 h after tracheal injury in the BAS group compared with the control group (Fig. 2i). Western blot analysis revealed that expression of cGAS,

https://doi.org/10.1038/s41467-024-55170-5

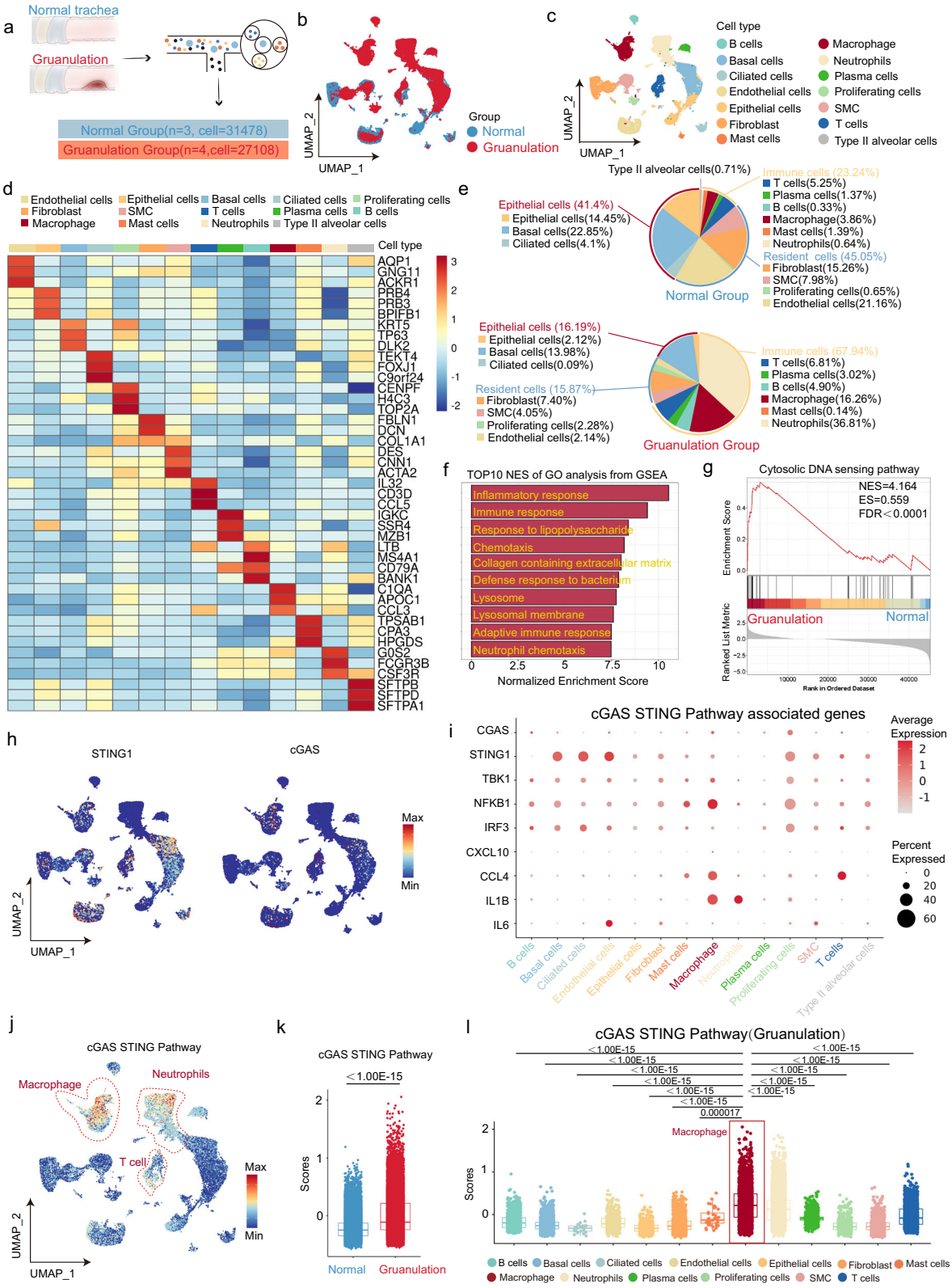

STING, and phosphorylation of STING, P65, and TBK1 were elevated at 24 h post-tracheal injury compared with the control group (Fig. 2j). To ascertain the function of the free dsDNA receptor cGAS in the context of BAS, the RU.521 cGAS inhibitor was administered to the mice (Fig. 2k). Following the administration of RU.521, granulation growth was effectively alleviated, and the thickness of the tracheal LP layer was significantly reduced (Fig. 2l, m). In addition to cGAS, the AIM2 inflammasome which also is activated by dsDNA[22]. Transcriptome sequencing data (Supplementary Fig. 3a) showed the low mRNA expression of AIM2 in the sham and BAS trachea tissue. WB also showed the low protein expression of AIM2 in the both sham and BAS trachea tissue (Supplementary Fig. 3b, c). In sc-RNA seq, we found that AIM2 was also low expression in macrophages (Supplementary Fig. 3d, e). Above data suggested that AIM2 might not function in the

Fig. 1 | Expression of the cGAS-STING pathway in BAS patients by single-cell RNA sequencing. a Schematic overview of the experimental design. Single-cell RNA sequencing of Normal group ($n = 3$, cell=31,478) and Granulation group ($n = 4$, cell=27108)**. b** UMAP visualization of Normal group and Granulation group (58586 cells in total). **c** UMAP visualization of 14 cell types (58586 cells in total). **d** Heatmap of expression for three representative marker genes of each cell type. **e** Pie chart of the total proportion of each cell type identified in Normal group and Granulation group. **f** GSEA analysis of increasingly expressed genes showing TOP 10 of enriched GO terms in Granulation group compared with Normal group. **g** GSEA analysis showing significant enrichment of gene sets associated with cytosolic DNA sensor pathway in Granulation group compared with Normal group. **h** UMAP visualization of *STING* and *cGAS* expression in all clusters. **i** Dot plot showing the expression of cGAS-STING pathway 9 associated genes (*cGAS*, *STING*, *TBK1*,*NFKB1*, *IRF3*, *CXCL10*,*CCL4*,*IL1B*,*IL6*) in all clusters. **j** UMAP visualization of cGAS-STING pathway score in all clusters. **k** Box Plot showing the cGAS-STING pathway score in Normal group ($n = 31,478$ cells) and Granulation group ($n = 27,108$ cell). **l** Box Plot showing the cGAS-STING pathway score in all clusters of Granulation group: B cells ($n = 1329$), basal cells ($n = 3790$), ciliated cells ($n = 25$), endothelial cells ($n = 580$), epithelial cells ($n = 574$), fibroblasts ($n = 2004$), mast cells ($n = 39$), macrophages ($n = 4409$), neutrophils ($n = 9977$), plasma cells ($n = 819$), proliferating cells ($n = 619$), SMCs ($n = 1097$) and T cells ($n = 1846$). *n* represents the number of cells in cluster. In (**k, l**), box bounds shows 25th and 75th percentiles, whiskers shows 25th percentiles minus 1.5*IQR(Interquartile Range, the value is 75th percentiles minus 25th percentiles) to 75th percentiles plus 1.5*IQR and box center shows the median.The two-sided Mann Whitney test was used in (**k**). One-way ANOVA analysis followed by Duncan multiple- range test was used in (**l**). Source data are provided as a Source Data file.

BAS progress. Together, these data suggested that free dsDNA is present in the trachea of patients with BAS and in a mouse model of BAS. Moreover, free dsDNA leads to the activation of the cytoplasmic DNA-sensitive cGAS–STING pathway in the trachea after tracheal injury in mice. In addition, inhibition of the DNA receptor cGAS effectively alleviates the symptoms of BAS.

STING is expressed at different stages of BAS

Considering that STING is widely expressed in haematopoietic cells (macrophages, T lymphocytes, and dendritic cells) and non-haematopoietic cells (endothelial cells, epithelial cells, and fibroblasts)[23], STING expression was analysed at different stages of BAS. Mfuzz analysis of the RNA-seq data revealed high expression of *cGAS* and *STING* at 24 h, with a decreasing trend in expression at 7 days after tracheal injury (Supplementary Fig. 2c). Immunofluorescence was used to analyse the phosphorylation status of STING in macrophages and fibroblasts during the different periods of BAS. In the early inflammatory phase of BAS, the level of STING phosphorylation was further increased in macrophages, but with the progression of BAS, there was a gradual increase of the level of STING phosphorylation in fibroblasts (Fig. 3a). During the inflammatory phase, the trachea was infiltrated with many inflammatory cells, such as macrophages, 24 h after tracheal injury (Supplementary Fig. 7a, b). The proportion of STING-positive macrophages among $CD45^+$ (pan-leukocyte marker) cells was analysed, which revealed that the number of STING-positive macrophages increased during the inflammatory phase of airway stenosis in the BAS group compared with the control group (Fig. 3b, c). Moreover, immunofluorescence analysis revealed many $STING^+F4/80^+$ coexpressing cells in the trachea of mice in the BAS group, whereas such cells were rarely found in the control group (Fig. 3d). The immunohistochemical results suggested that STING was expressed in both epithelial cells and fibroblasts from granulation tissue in the trachea of BAS mice at the granulation phase on Day 7 (Fig. 3e). Moreover, the immunofluorescence analysis revealed that there were STING + SMA+ and STING + E-cad+ coexpressing cells in the trachea of the mice in the BAS group, whereas such cells were rarely found in the control group (Fig. 3f, g). STING is strongly linked to the development of fibrotic diseases, and the activation of STING has been demonstrated to facilitate the activation of fibroblasts[24,25]. However, it remains unknown whether STING is activated within fibroblasts and is associated with the fibrotic process in BAS. Next, the fibroblast clusters in the scRNA-seq data were analysed (Supplementary Fig. 4a), which demonstrated that the expression levels of the COL1, FAP, TGFB1, and FN1 fibroblast activation genes were elevated in the fibroblast clusters of the granulation group compared with those of the normal group (Supplementary Fig. 4b). The cGAS-STING pathway score was greater in the fibroblast clusters of the granulation group than in those of the normal group (Supplementary Fig. 4c). After fibroblast stimulation via the transfection of mouse tracheal DNA, the level of STING phosphorylation was significantly increased, and the levels of fibroblast-related markers, including collagen I and SMA, were increased in fibroblasts (Supplementary Fig. 4d, e). When *STING* was knocked down in fibroblasts via siRNA (Supplementary Fig. 4f, g), DNA stimulation failed to promote the activation of fibroblasts (Supplementary Fig. 4h, i). Taken together, these results showed that STING is expressed at acute and chronic inflammation stages of BAS.

Suppression of STING attenuates the development of BAS

To confirm the effect of the cGAS-STING pathway on the progression of BAS, mice were treated with the C176 STING inhibitor (Fig. 4a). Western blot analysis revealed the ability of C176 to reduce the expression of STING and the level of STING phosphorylation (Fig. 4b).On the 7th day after modelling, the BAS group of mice treated with C176 presented significantly less development of granulation tissue, proliferation of the airway epithelium, collagen deposition, and degree of fibrosis compared to the BAS group of mice treated with PBS (Fig. 4c). Moreover, quantitative assessment of LP thickness revealed a thinner LP in C176-treated BAS mice than in PBS-treated BAS mice (Fig. 4d). In addition, we administered the drug 24 h after tracheal injury and found the same protective effect (Supplementary Fig. 5a, b). The same phenomenon was observed in *STING* KO mice at 7 days after tracheal scraping in which the degree of granulomatous hyperplasia in the trachea was significantly lower in the BAS group than in the WT group (Fig. 4e).Histopathologic analysis revealed reduced LP thickness in *STING* KO mice compared with WT mice on the 7th day after modelling (Fig. 4f). Masson's trichrome staining revealed that *STING* knockout mice with BAS expressed fewer collagen fibers than wild-type mice (Fig. 4g, h). Micro-CT scans of wild-type mice and *STING* KO mice in the control group revealed no tracheal stenosis (Fig. 4j, k). In contrast, on the 7th day after modelling, the wild-type mice and *STING* KO mice exhibited the formation of discernible protrusions within the tracheal lumen (Fig. 4j, k). This aberration was indicative of localized narrowing at the site of injury, which was readily apparent upon imaging analysis. Notably, micro-CT scans revealed that the severity of luminal constriction was markedly lower in *STING* knockout mice than in their wild-type counterparts (Fig. 4i). These results suggested that the inhibition of STING reduces the progression of airway stenosis and may also inhibit the progression of fibrosis.

Macrophage STING expression in BAS is associated with inflammation

At present, the main clinical treatment for BAS is the removal of granulation tissue under bronchoscopy, but this can cause secondary stenosis. Therefore, early intervention may effectively alleviate the proliferation of granulation tissue. The present study demonstrated that STING was expressed in the early acute inflammatory stage of BAS and in the later chronic inflammatory stage (granulation hyperplasia). STING has been shown to be strongly associated with inflammation[26]. As shown by the heatmap of key DEGs, *STING* and inflammatory genes were highly expressed at 24 h after tracheal injury in the treated mice

https://doi.org/10.1038/s41467-024-55170-5

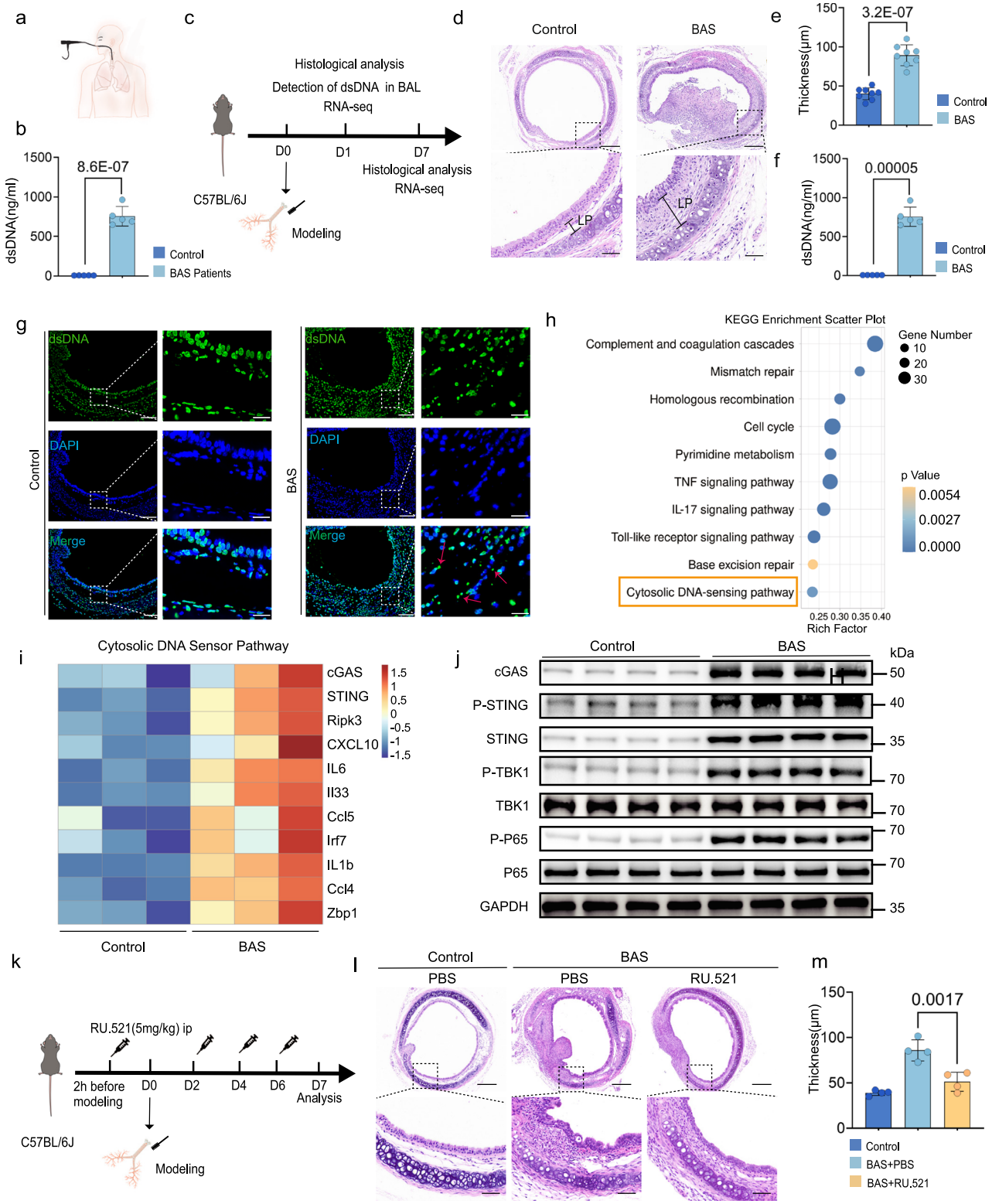

compared with the control mice (Fig. 5a). To investigate the role of STING in the inflammatory phase of airway stenosis, mice were treated with C176 (Fig. 5b). Compared with those of the BAS group treated with PBS, the wheezing symptoms of the BAS group treated with C176 improved during the inflammatory phase of airway stenosis, and the HE staining results revealed that the degree of inflammatory oedema in the airways of the BAS group treated with C176 also improved (Fig. 5c). In the early inflammatory stage, the airway injury caused airway inflammation and edema, resulting in tracheal stenosis and wheezing. Noninvasive pulmonary function test showed that C176 could effectively reduce the inspiratory time of the mice after tracheal injury, thereby alleviating the wheezing symptoms of the mice (Fig. 5d). Moreover, the qRT-PCR results suggested that the expression of *IL6*, *IL1β* and *CXCL10* in the BAS group treated with C176 was significantly lower than that in the BAS group treated with PBS (Fig. 5e). At the protein level, the multifactorial assay similarly suggested that the expression of inflammatory factors and inflammation-associated chemokines was reduced after airway injury in mice injected with C176

Fig. 2 | cGAS-STING signalling is activated in mouse tracheal upon injury. **a** Schematic diagram of tracheal lavage of the patient. **b** Quantification analysis of dsDNA in tracheal lavage fluid in control group ($n = 5$) and BAS patients' group ($n = 5$). **c** Schematic diagram describing experimental strategies in mice with benign airway stenosis. **d** H&E staining showing Intratracheal and LP conditions in control and BAS mice at 7th day. Scale bars indicate 200μm and 50μm.**e** Quantitative analysis of LP thickness in control group and BAS group ($n = 8$ mice per group). **f–j** Tracheal tissues were collected from mice with BAS at 24 h after tracheal injury. **f** Quantitative detection of dsDNA in tracheal lavage fluid of mice in control group and BAS group (n = 5 mice per group). **g** Representative tracheal immunofluorescence images of dsDNA(green) in the BAS group and control group. Scale bars indicate 100μm and 20 μm ($n = 3$ mice per group). **h** Kyoto Encyclopedia of Genes and Genomes (KEGG) analysis showing that tracheal injury upregulated genes involved in several biological process. **i** Heatmap showing that the BAS group upregulated genes involved in cytosolic DNA sensor pathway compare to control group ($n = 3$ mice per group). **j** Western blot analysis showing the levels of cGAS, P-STING, STING, P-TBK1, TBK1, P-P65, and P65 in the trachea of BAS group and control group ($n = 4$ mice per group) at 24 h. **k** Schematic of Ru.521(5 mg/kg, ip) administration in mice. **l** H&E staining showing Intratracheal and LP conditions in control and BAS mice at 7th day. Scale bars indicate 200 μm and 50 μm.**m** Quantitative analysis demonstrated decreased lamina propria thickness in BAS group treated with Ru.521 compared to BAS group treated with PBS ($n = 4$ mice per group). Data are presented as the mean ± SEM. A two-sided student's T-test was used in (**b**, **e**, **f**). hypergeometric test was used in (**h**). One-way ANOVA analysis followed by Tukey post hoc multi-comparison test was used in (**m**). Source data are provided as a Source Data file.

(Fig. 5f). The process of wound healing, proinflammatory macrophages play an important role, as they produce proinflammatory cytokines, such as TNF-a and IL6 and other mediators that promote wound healing[27].The macrophage clusters in the scRNA-seq data were separately analysed, with 1216 cells in the normal group and 4,409 cells in the granulation group (Fig. 5g). The macrophages were further classified into seven functional clusters (Mc1-Mc7) (Fig. 5h). Of these, the Mc5, Mc6, and Mc7 clusters were present in both groups. The normal group had predominantly M2 clusters, and the granulation group had predominantly Mc1 clusters and a small number of Mc3 and Mc4 clusters (Fig. 5i). The Mc1 cluster had the highest percentage of DEGs in the granulation group, with signature genes corresponding to lipid metabolism, the regulation of inflammatory responses, and the promotion of tissue repair. The top 5 biological processes according to the GO analysis were also predominantly related to inflammation, immunity, and lipid metabolism (Fig. 5j, k). The Mc2 cluster, which constituted the majority of the normal group, highly expressed *MRC1*, suggesting that it is a tissue-retained macrophage, and GO analyses revealed a predominantly translational correlation (Fig. 5j, k). The Mc3 and Mc4 clusters present in the granulation group presented proinflammatory features, and the marker genes were mainly early inflammatory genes (*IL1B*) and warning proteins (*S100a8* and *S100a9*). GO analyses of the Mc3 and Mc4 clusters indicated that these clusters were associated mainly with inflammation and immunity. In addition, the *VCAN* marker gene suggested that the Mc3 and Mc4 clusters were located mainly in the extracellular matrix (Fig. 5j, k). *IRF4*, which is a macrophage polarization gene, was marker gene for the M5 cluster, suggesting that this cluster may polarize towards pro-repair macrophages (Fig. 5j, k)[28]. The Mc6 cluster showed antigen processing activity and expressed *HLA-DQA1*, *LAMP3*, and *HLA-DOB*, which are linked to antigen presentation, and the GO terms included antigen processing and presentation (Fig. 5j, k). Mc7 exhibited reparative and collagenic activity, and it expressed genes associated with collagenous ECM (*COL1A1* and *COL4A1*) and tissue repair-related GO terms (cell adhesion and cell migration) (Fig. 5j, k). Mc7 also expressed a vascular repair-related gene (*VWF*), suggesting that it is also involved in neovascularization in granulation tissue (Fig. 5j). The cGAS–STING pathway score was assessed across clusters, which revealed higher scores for Mc1, Mc3, and Mc4 (Fig. 5l). In addition, several inflammatory factors, such as *IL6*, *IL1β*, and *CXCL10*, were also mainly concentrated in the Mc1, Mc3, and Mc4 clusters (Fig. 5m). Because Mc1, Mc3, and Mc4 macrophages were associated mainly with inflammation (Fig. 5j, k), the macrophage clusters with high cGAS–STING pathway scores may be associated with inflammation. Overall, these findings suggested that in the early stages of airway injury, STING activation in macrophages within the airway promotes inflammatory factor expression.

Macrophages promote fibroblast activation via the IL6-STAT3 axis

Gene set enrichment analysis (GSEA) using MSigDB hallmark gene sets revealed that compared with the normal group, the granulation group was enriched predominantly in inflammation-associated pathways, cell growth-related pathways, and oxidative stress-related pathways (Fig. 6a). Among these pathways, the IL6-STAT3 pathway was associated with granulation (Fig. 6b) has been shown to be associated with fibrosis[29,30]. STAT3 has recently been reported to be highly expressed in the tracheal granulation tissue of patients with BAS[31]. Next, the present study analysed from the scRNA-seq data and revealed that the JAK-STAT pathway was associated primarily with fibroblasts (Fig. 6c). Immunohistochemistry analysis indicated that granulation tissue from patients with BAS highly the level of STAT3 and STING phosphorylation compared with normal airways (Fig. 6d). The high cGAS–STING pathway score was focused mainly on immune cells, such as macrophages, T cells, and neutrophils (Fig. 2h). Compared with T cells and neutrophils, macrophages strongly interact with fibroblasts according to CellPhoneDB ligand–receptor analysis (Fig. 6e). The *IL6* expression levels were assessed via scRNA-seq, which revealed that *IL6* expression was increased in macrophages, SMCs, fibroblasts, and endothelial cells (Supplementary Fig. 6a). Cells expressing both *STING* and *IL6* were assessed in the four clusters, which indicated that the strongest correlation between *STING* and *IL6* expression was in the macrophage cluster (Supplementary Fig. 6b). To investigate the relationship of macrophages with fibroblasts and mice were treated with clodronate liposomes (Fig. 6f). Flow Cytometry analysis suggested that during the inflammatory phase, macrophage infiltration was significantly greater in the BAS group with injected with PBS than in the control group injected with PBS, but the percentage of macrophages in the BAS group clearly decreased after clodronate liposome injection compared with that in the PBS group (Supplementary Fig. 7c). The histological results suggested that after Clodronate Liposomes injection, granulomatous proliferation in the trachea of mice in the BAS group was significantly inhibited compared with that in PBS injection group on the 7th day (Fig. 6g). Moreover, the LP thickness in the BAS group treated with Clodronate Liposomes was significantly smaller than that in the BAS group treated with PBS (Fig. 6h). The potential therapeutic benefits of inhibiting of the fibrotic process in BAS on the 14th day after tracheal injury were explored. The BAS group treated with PBS presented of fibrous scarring of tracheal rings, but the BAS group treated with Clodronate Liposomes did not have excessive fibrous deposition at the site of tracheal injury, but instead had a state of just-injured trachea (Fig. 6g). Moreover, the LP thickness in the BAS group treated with Clodronate Liposomes was still lower than that in the BAS group treated with PBS (Fig. 6h). Micro-CT data suggested that the hyperplastic neoplastic organisms in the trachea of the mice were significantly smaller after clodronate injection (Fig. 6i, j). Next, the degree of tracheal stenosis at the horizontal level was analyzed, which revealed that the degree of stenosis in the BAS group treated with Clodronate Liposomes was less than that in the BAS group treated with PBS (Fig. 6k). Thus, these results suggested that macrophage depletion attenuates the progression of BAS, suggesting that macrophages may play an important role in fibrosis in BAS. To investigate the role of macrophages in fibrosis in BAS, RNA-seq was conducted on mice

https://doi.org/10.1038/s41467-024-55170-5

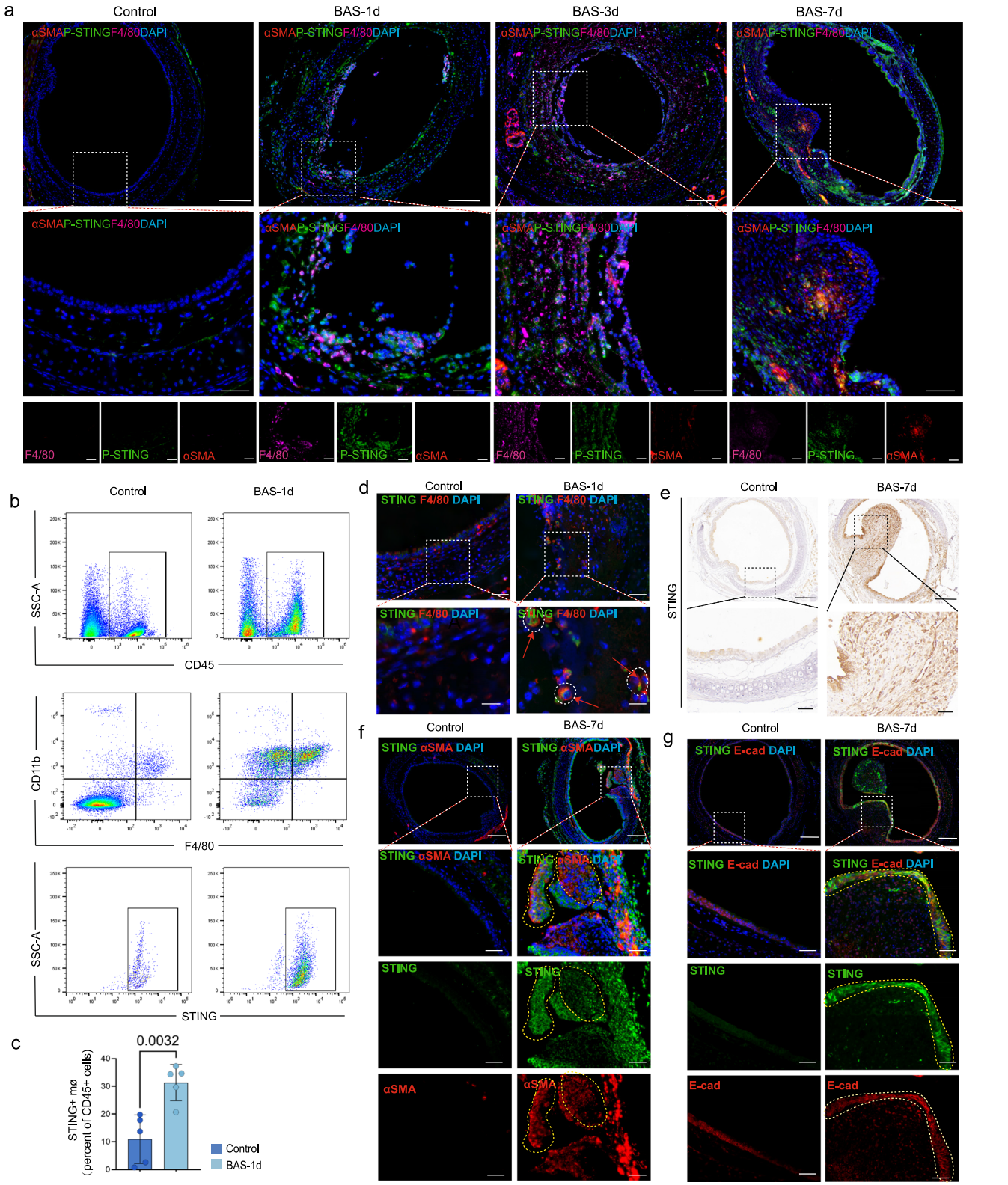

7 days after modelling, as well as on the Clodronate Liposomes-injected group of mice 7 days after modelling. Gene Ontology (GO) analysis of the transcriptome revealed that the enriched DEGs, such as genes related to extracellular matrix organization, cell adhesion, collagen trimers, collagen-containing extracellular matrix, and extracellular matrix structural constituents conferring tensile strength, in the BAS group treated with PBS and treated with clodronate liposomes were predominantly associated with fibrosis compared with those in the control group; however, the degree of enrichment was lower in the clodronate liposome-injected group than in the PBS-injected group (Supplementary Fig. 8a). A heatmap of the RNA sequencing results indicated that the expression of inflammation-related genes and fibrosis-related genes was significantly upregulated compared with that in the control group, but the degree of upregulation in the BAS group treated with Clodronate Liposomes was lower than that in to the BAS group treated with PBS (Supplementary Fig. 8b). GSEA of KEGG

Fig. 3 | STING was expressed at different stages of BAS. a Tracheal specimens were collected from control group of mice and BAS group of mice at 24 h, 3 days, and 7 days after modeling, and representative immunofluorescence images of P-STING (green), macrophages (marked with F4/80, pink), fibroblasts (marked with aSMA, red) in mice tracheal tissues. Scale bars indicate 200 μm and 50 μm ($n = 3$ mice per group). **b**–**d** Tracheal tissues were collected from mice with BAS at 24 h after tracheal injury. **b**, **c** Flow cytometry plots demonstrate percentage of STING$^+$ macrophages in tracheal leukocytes (CD45$^+$ cells), and the results showed that the percentage was significantly higher in the BAS group compare to control group ($n = 5$ mice per group). **d** Representative tracheal immunofluorescence images of STING(green), and macrophages (marked with F4/80, red) in mice ($n = 4$ mice per group). Scale bars indicate 50 μm and 20 μm. Red arrows indicate STING$^+$ macrophages. **e**–**g** Tracheal tissues were collected from mice with BAS at 7 d after tracheal injury. **e** Immunohistochemical results suggested that STING expressing in the trachea of BAS mice at the granulation stage on the 7th day ($n = 3$ mice per group). Scale bars indicate 200 μm and 50 μm. **f** Representative tracheal immunofluorescence images of STING (green), and fibroblasts (marked with aSMA, red) in mice ($n = 3$ mice per group). Yellow dashed line: Areas of co-expression of STING and aSMA. Scale bars indicate 200 μm and 50 μm. **g** Representative tracheal immunofluorescence images of STING (green), and epithelial cells (marked with E-cad,red) in mice ($n = 3$ mice per group). Yellow dashed line: Areas of co-expression of STING and E-cad. Scale bars indicate 200μm and 50μm. Data are presented as the mean ± SEM. A two-sided student's T-test was used in (**c**). Source data are provided as a Source Data file.

gene sets revealed reduced enrichment of the cytosolic DNA-sensing pathway, the NFkb pathway, and pathways related to tissue repair, such as ECM receptor interaction and cell adhesion, following clodronate liposome administration (Supplementary Fig. 8c). Notably, Masson staining results revealed that the BAS group treated with Clodronate Liposomes presented a lower level of collagen fib redeposition compared to the BAS group treated with PBS (Fig. 6l, m). The immunofluorescence results suggested that the expression levels of SMA and collagen-1 were markedly elevated in the BAS group; however, the expression levels of SMA and collagen-1 in the BAS group treated with clodronate liposomes were lower than those in the BAS group treated with PBS (Fig. 6n, o). the present study explored the mechanism of macrophages promoting fibroblast activation. Gene set enrichment analysis of the transcriptional changes via curated hallmark pathways revealed strong upregulation of the IL6-STAT3 pathway, indicating a high degree of enrichment in mice with BAS (Supplementary Fig. 9a). Subsequently, mice were treated with STATTIC, an inhibitor of STAT3, on mice (Supplementary Fig. 9b). HE staining revealed that granulation proliferation in the trachea was blocked and the thickness of LP was significantly reduced in the BAS group treated with STATTIC compared with the BAS group treated with PBS (Supplementary Fig. 9c,d). These data suggested that STAT3 plays an important role in the progression of BAS. The RNA-seq results indicated that the IL6-STAT3 pathway was less enriched in the BAS group treated with Clodronate Liposomes than in the BAS group treated with PBS (Fig. 6p) Next, the role of macrophages on STAT3 was investigated. After macrophage depletion, the expression levels of IL6 and the level of STAT3 phosphorylation in the trachea of BAS mice were significantly lower than those in the BAS group treated with PBS (Fig. 6q, r). To assess the effect of IL6 on BAS, mice were treated with an IL6 neutralizing antibody and exogenous IL6 supplementation (Supplementary Fig. 9e). HE staining revealed that the proliferation of granulation tissue was alleviated by the use of an IL6 neutralizing antibody, whereas supplementation with exogenous IL6 exacerbated the growth of the granulation tissue (Supplementary Fig. 9f). In addition, the thickness of the LP layer also decreased and increased with IL6 antagonism and supplementation, respectively (Supplementary Fig. 9g). Immunofluorescence analysis revealed that the use of an IL6 neutralizing antibody reduced the level of STAT3 phosphorylation and fibroblast activation, whereas IL6 supplementation promoted he level of STAT3 phosphorylation expression and fibroblast activation (Supplementary Fig. 9h, i).These data revealed that macrophage depletion is beneficial for alleviating the fibrotic process of BAS, and that the interaction between macrophages and fibroblasts is mediated through the IL6-STAT3 signalling pathway.

Tracheal DNA activates the STING pathway in macrophages thereby promoting fibroblast activation via the IL6-STAT3 axis

The dsDNA released by cell death can activate STING in macrophages, promoting the release of inflammatory factors[32]. The present study confirmed that there is substantial release of dsDNA after tracheal injury and numerous highly expressed pathways associated with the repair of DNA damage after 24 h after tracheal injury (Fig. 7a). The γ H2AX marker, which is commonly associated with DNA damage, was identified 24 h after the modelling process and was expressed mainly in the tracheal epithelium after injury (Fig. 7b). Immunofluorescence staining showed that the colocalization macrophages marker F4/80 with free dsDNA, cGAS as well as P-STING in the injured tracheal (Fig. 7c). To investigate whether free dsDNA acts to recruit macrophages after tracheal injury, mice were treated with DNase I (Supplementary Fig. 10a). The dsDNA content of the mouse tracheal lavage fluid decreased significantly after the use of DNase I (Supplementary Fig. 10b). Moreover, the degree of inflammation and oedema after tracheal injury in mice was also improved with the use of DNase I (Supplementary Fig. 10c). Immunofluorescence and flow cytometry analyses indicated that macrophage infiltration in the trachea of mice was significantly reduced after the use of DNase I (Supplementary Fig. 10d–g). Next, the death epithelial cell supernatant (DECS) was used to culture BMDMs (Fig. 7d). After ultraviolet-induced epithelial cell death, the DECS contained a large amount of dsDNA (Fig. 7e, f). Moreover, the level of STING phosphorylation in BMDMs was significantly elevated after 24 h of culture with DECS (Fig. 7g, h). Tracheal DNA was obtained from mice 24 h post-modelling, followed by the activation of BMDMs (Fig. 7i). Western blot analysis revealed increased the level of STING phosphorylation in BMDMs after transfection of tracheal DNA (Fig. 7j, k). Moreover, Moreover, immunofluorescence analysis revealed that the expression level of P-STING in BMDMs increased after transfection of the tracheal DNA, whereas it decreased after treatment with DNase I (Fig. 7l, m). The ELISA results demonstrated that the concentration of IL6 in the culture supernatant of BMDMs was significantly increased after the transfection of tracheal DNA (Fig. 7o). The qRT-PCR analysis suggested that BMDMs transfected with DNA expressed significantly lower levels of *IL6* after treatment with C176, an inhibitor of STING (Fig. 7p). Together, these findings suggested that the inhibition of STING was also able to reduces the level of STAT3phosphorylation. Immunofluorescence analysis suggested that in the trachea of *STING* KO mice with BAS, the expression of IL6 and STAT3 was significantly lower than that in the trachea of wild-type with BAS (Fig. 7q, r). Therefore, these findings suggested that the inhibition of STING in macrophages is followed by a decrease in IL6 expression, which inhibits fibrosis by suppressing STAT3 activation in fibroblasts. Subsequently, BMDM were cocultured with fibroblasts and tracheal DNA was used to activate STING in BMDMs (Fig. 7s). Compared with those in the control group, immunofluorescence analysis indicated that the expression of P-STAT3 and αSMA in fibroblasts in the coculture group increased, but the expression of P-STAT3 and αSMA was reduced after the addition of C176 to the coculture of BMDMs and fibroblasts transfected with DNA (Fig. 7t, u). These results suggested that dsDNA released after tracheal injury activates the STING pathway in macrophages, which promotes the expression of the IL6 inflammatory factor, which further activates STAT3 expression in fibroblasts, thereby promoting fibroblast activation to accelerate fibrosis in patients with benign airway stenosis.

https://doi.org/10.1038/s41467-024-55170-5

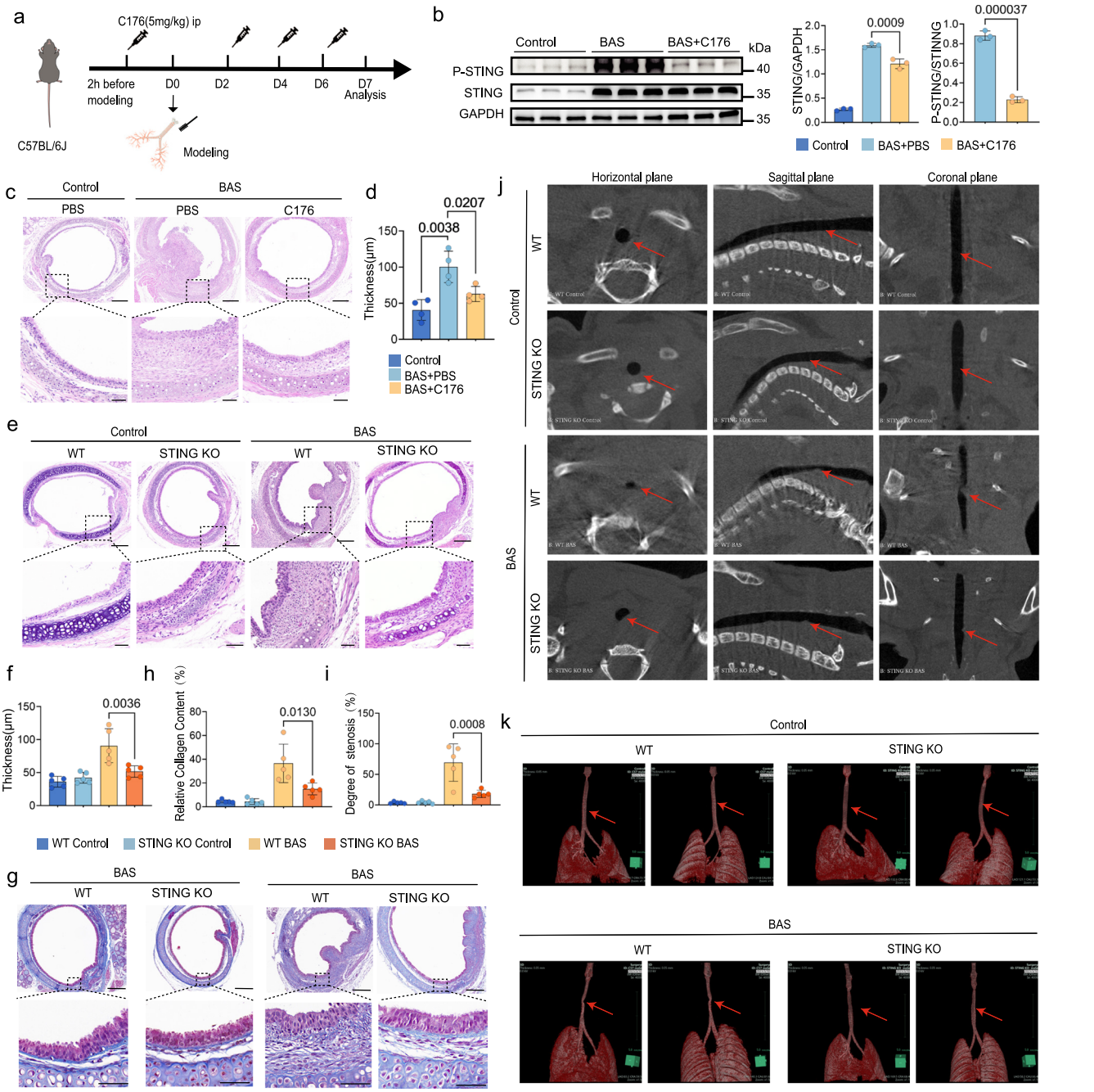

Fig. 4 | Suppression of the STING attenuates the development of BAS. **a** Schematic of C176 administration in mice. **b** Western blot analysis showing the P-STING and STING expression in mouse trachea at 24 h after modeling in control group, BAS group treated with PBS and BAS group treated with C176 ($n = 3$ mice per group). **c** H&E staining showing Intratracheal and lamina propria conditions in control group, BAS group treated with PBS and BAS group treated with C176 ($n = 4$ mice per group). Scale bars indicate 200 μm and 50 μm. **d** Quantitative analysis demonstrated decreased lamina propria thickness in BAS group treated with C176 compared to BAS group treated with PBS ($n = 4$ mice per group). **e** H&E staining showing Intratracheal and lamina propria conditions in WT control group,STING KO control group, WT BAS group, STING KO BAS group ($n = 5$ mice per group). Scale bars indicate 200 μm and 50 μm. **f** Quantitative comparison of tracheal LP showed reduced thickness at STING KO BAS group compare to WT BAS group ($n = 5$ mice per group). **g**, **h** Tracheal sections stained with Masson trichromatic staining of different groups of mice, and relative collagen content were reduced in STING KO BAS group compare to WT BAS group ($n = 5$ mice per group).Scale bars indicate 200 μm and 50 μm. **i** The CT diagram of the area of tracheal stenosis measured by SYNPASE 3D, and results showed that the area of tracheal stenosis in STING KO BAS group was significantly smaller than that in WT BAS group ($n = 5$ mice per group). **j** Micro CT scans of different groups in Horizontal, Coronal and Sagittal plane with red arrows indicating the stenosis site. **k** SYNPASE 3D reconstruction of mouse trachea with red arrows indicating the stenosis site. Data are presented as the mean ± SEM. Two-sided student's T-test were used in (**b**). One-way ANOVA analysis followed by Tukey post hoc multi-comparison test was used in (**b**, **d**). Two-way ANOVA analysis followed by Tukey post hoc multi-comparison test was used in (**f**, **h**, **i**). Source data are provided as a Source Data file.

Discussion

In recent years, with the increase in critical care ambulances, endotracheal intubation, tracheotomy and other manipulations, the incidence of BAS has gradually increased. Although the current respiratory interventions control symptoms in the short term, they carry a risk of restenosis. Therefore, identifying therapeutic targets to prevent BAS is imperative. The present study revealed that the inhibition of STING reduces the degree of fibrosis associated with BAS and improves patient

https://doi.org/10.1038/s41467-024-55170-5

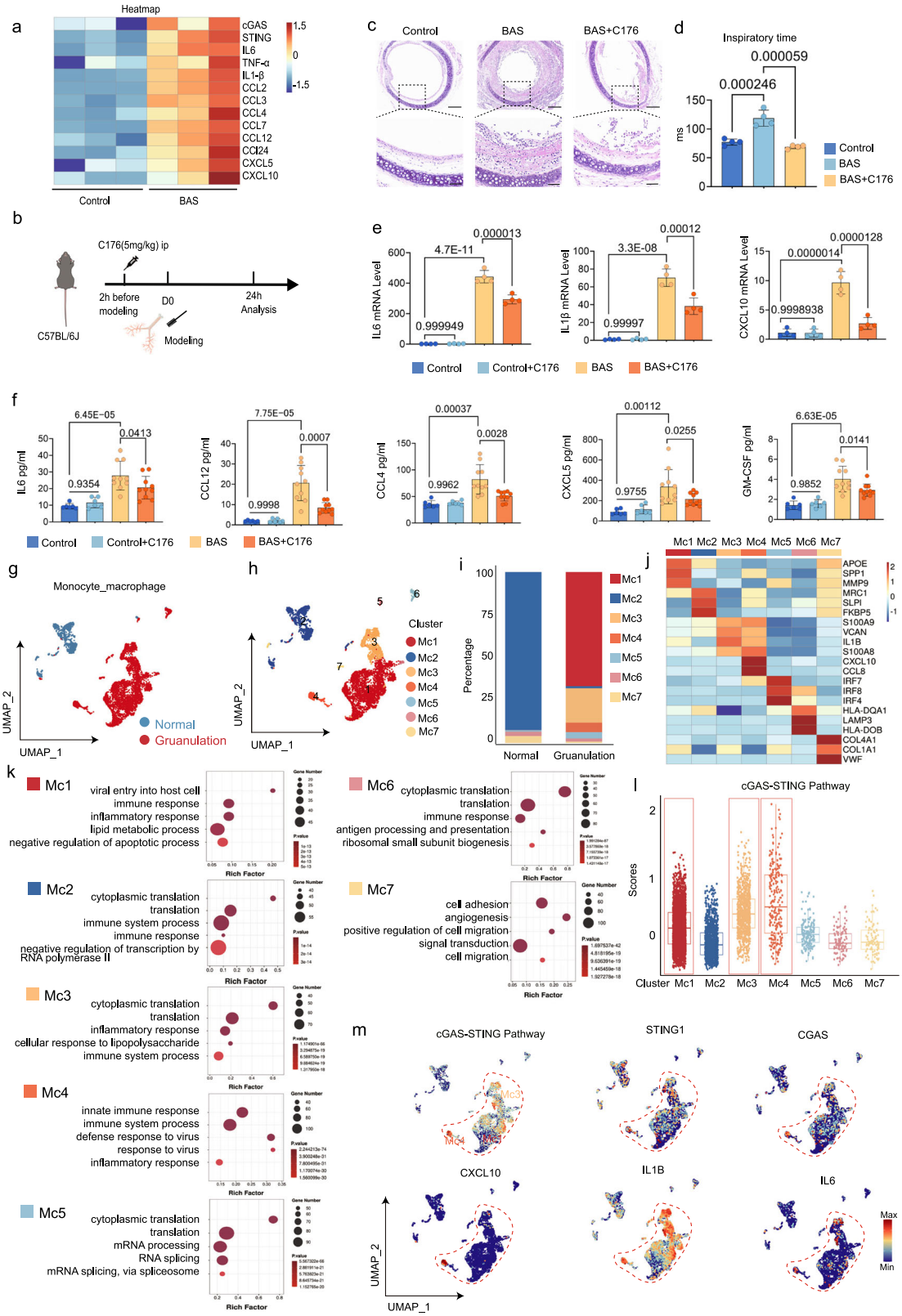

prognosis. Mechanistically, this improvement due to the release of dsDNA from tracheal injury, which activates STING-promoted IL6 release from infiltrating macrophages during the inflammatory phase of benign airway stenosis. Increased IL6 further activates STAT3 in fibroblasts, thereby promoting fibrosis. The comprehensive research strategy and process was shown in Fig. 8. These findings suggest that the cGAS–STING pathway is a critical factor involved in BAS.

The repair process after tracheal injury has similar characteristics to that of other soft tissue and organ injuries, and it involves four procedural stages, namely, haemostasis, inflammation, proliferation, and remodelling[33]. Dysregulation at any stage can lead to hyperplasia of scar granulation. The progression of benign airway stenosis involves the activation of certain immune cells, cytokines and a range of signalling pathways. Hence, BAS is now being recognized as a

Fig. 5 | STING expression in macrophages in BAS is associated with inflammation. a Heatmap showing that the BAS group upregulated genes involved in cGAS,STING and inflammation factors compare to control group at 24 h after tracheal injury ($n = 3$ mice per group). **b**–**f** Mice were divided into three groups: control, BAS + PBS and BAS + C176. **b** Schematic of C176 administration in mice. **c** Representative images of H&E staining in different groups. Scale bars indicate 200 μm and 50 μm. **d** Quantitative comparison of lung function indices (Inspiratory time) in different groups ($n = 4$ mice per group). **e** mRNA levels of *Il6*, *Il1β* and *Cxcl10* in trachea from different groups ($n = 4$ mice per group). **f** Protein levels of inflammation factors (IL6,CCL12,CCL4,CXCL5 and GM-CSF)in trachea from different groups ($n = 6$ mice per control group, $n = 8$ mice per BAS group). **g**–**m** sc-RNA seq analysis of macrophage clusters. **g** UMAP visualization of macrophage clusters in Normal group (1216 cells in total) and Granulation group (4409 cells in total). **h** UMAP visualization of Seven types of macrophages (5625 cells in total). **i** Barplot of the percentage of each type in Normal group and Granulation group. **j** Heatmap of expression for three representative marker genes of each cell type. **k** Dot plot of the enriched Gene ontology (GO) biological processes of highly expressed genes in each cluster. Dot size corresponds to the proportion of cells within the group expressing each gene, and dot color correspond to GO enrichment *p*-value. **l** Box Plot showing the cGAS-STING pathway score in all clusters:Mc1 ($n = 2945$), Mc2($n = 1176$), Mc3 ($n = 881$), Mc4 ($n = 245$), Mc5 ($n = 172$), Mc6 ($n = 110$), Mc7 ($n = 96$). n represents the number of cells in cluster. **m** UMAP visualization of cGAS-STING pathway score and the expression of *STING*,*cGAS*,*IL1B*,*IL6* and *CXCL10* in all clusters. In (**l**), box bounds shows 25th and 75th percentiles, whiskers shows 25th percentiles minus 1.5*IQR to 75th percentiles plus 1.5*IQR and box center shows the median. Data are presented as the mean ± SEM. One-way ANOVA analysis followed by Tukey post hoc multi-comparison test was used in (**d**, **e**). Kruskal waliis test used in (**f**). Hypergeometric test was used in (**k**). Source data are provided as a Source Data file.

fibroinflammatory event triggered by immune alterations[34]. The cGAS-STING pathway plays an essential role in intrinsic immunity, and a previous study has confirmed that dsDNA released after injury exacerbates inflammation and fibrosis by activating cGAS-STING[35]. The present findings indicated that free dsDNA is present in the trachea of BAS patients and mice after tracheal scraping with a small brush. Additionally, the RNA sequencing results suggested that there is an enrichment of genes related to DNA damage in the early stages of BAS. Therefore, the present findings suggested that the dsDNA produced following tracheal injury may serve as the initiator of the cGAS–STING pathway. While there are no studies that directly link the cGAS–STING pathway to BAS, it has been demonstrated to be involved in fibrotic processes in other organs and tissues[36]. Single-cell sequencing analysis of normal trachea and granulation tissue from BAS patients revealed that cGAS–STING pathway was activated in granulation tissue. Similarly, the present results revealed significant upregulation of cGAS–STING pathway expression in a mouse model of BAS. After the inhibition or knockout of *STING*, inflammation and fibrosis associated with airway stenosis are alleviated in mice. These results suggested that cGAS-STING signalling in macrophages is responsible for the acute inflammation phase and that cGAS-STING signalling in fibroblasts may be responsible for the chronic inflammation phase of granulation. Administration of C176 every other day may alleviate granulation by decreasing inflammation, suggesting that C176 may be a potential drug candidate for BAS.

The inflammatory phase is an important stage in the fibrotic process of benign airway stenosis. The purpose of this method is to remove pathogens and necrotic tissue to lay the foundation for tissue regeneration and repair. In the present study, the cGAS-STING pathway was highly activated during the inflammatory phase of BAS, and STING inhibitors were effective in alleviating airway inflammation. During the inflammatory phase of fibrosis, many inflammatory cells, such as neutrophils, macrophages, and lymphocytes, infiltrate. Macrophages play an important role in inflammatory phase by acting as scavengers, engulfing dead cells and debris in their surroundings while secreting a considerable quantity of cytokines (IL6, IL1and TNFα)[37]. Aberrant activation of the cGAS-STING pathway in macrophages has been reported to be associated with fibrosis-related diseases[38]. In the present study, the trachea was infiltrated with large numbers of STING-expressing macrophages during the inflammatory phase of BAS in mice. Similarly, scRNA-seq analysis revealed that a highly scored macrophage population of the cGAS-STING pathway was strongly associated with an inflammatory response. Therefore, these findings suggested that the expression of STING in infiltrated macrophages infiltrated during the inflammatory phase of benign airway stenosis is correlated with inflammation. In addition, stimulation of BMDMs with dsDNA from dead epithelial cells and from mouse trachea activated STING.

Fibroblasts are the key cellular effector cells for extracellular matrix deposition and reorientation in fibrotic diseases[39]. Interestingly, the present study detected STING-expressing fibroblasts in the trachea of BSA-treated mice at the chronic inflammation stage. Activation of STING in fibroblasts via the transfection of mouse tracheal DNA promoted fibrosis in fibroblasts, and this effect was inhibited by knocking down *STING*. Previous studies have indicated that during myocardial infarction (MI), stimulation of the cGAS–STING pathway in infiltrated macrophages can induce fibrosis of cardiac fibroblasts[18], suggesting that the same situation may exist within the BAS. Research has indicated that eliminating macrophages during the initial stages of inflammation can help minimize scar formation[27]. Consistent with this perspective, the present study detected significantly less fibrosis in mice with benign airway stenosis after depletion of mouse macrophages. RNA sequencing of mice and scRNA-seq data revealed that the fibrosis process may be affected through the IL6-STAT3 pathway. Although the IL6-STAT3 pathway has been shown to be associated with fibrotic disease[40],no studies have confirmed that this axis plays a role in BAS. In this study, the present study demonstrated that the level of STAT3 phosphorylation was highly in human tracheal granulation tissue, and that trachea fibrosis is attenuated in BAS mice after the inhibition of P-STAT3. In addition, the role of IL6 was explored in BAS. Tracheal fibrosis in BAS mice was alleviated or exacerbated after the use of an IL6-neutralizing antibody or supplementation with IL6. The present study also demonstrated that STING activation in macrophages promotes the release of IL6 and that the release of IL6 from macrophages was reduced after the use of STING inhibitors. In addition, the expression levels of P-STAT3 and fibrosis markers in fibroblasts were increased after coculturing tracheal DNA-stimulated BMDMs with fibroblasts. The present study also demonstrated that macrophages in granulation tissue presented significantly elevated levels of IL6 compared with those in normal tracheal tissue, and these macrophages presented high expression levels of *IL-1β* and *CXCL10* (Fig. 5m). Moreover, treatment with the C176 STING inhibitor resulted in a significant reduction in the expression of these cytokines (Fig. 5e), indicating the potential role of the cGAS-STING pathway in the development of BAS. Previous studies have established a strong correlation between IL-1β and various fibrotic diseases[41], and CXCL10 has been suggested to be crucial for the chemotaxis of immune cells. IL-1β has been implicated in inflammasome activation, and we found that AIM2 inflammasome may not play a role in BAS. In addition to AIM2 inflammasome, NLRP3 inflammasome and NLRP1 inflammasome are also activated IL-1β. So, we analyzed the transcriptome data of the trachea of BAS mice and found that NLRP3 and NLRP1 were highly expressed (Supplementary Fig. 3f). And in the sc-RNA seq data, IL-1β was highly expressed mainly in macrophages and neutrophils, where there was high expression of NLRP3 in macrophages and NLRP1 in neutrophils (Supplementary Fig. 3g). Therefore, the highly expressed IL-1β is not related to AIM2 in BAS, but is related to NLRP3 and NLRP1.And it has been confirmed that cGAS-STING pathway also leads to NLRP3 activation[42]. These findings suggest that IL-1β and CXCL10

https://doi.org/10.1038/s41467-024-55170-5

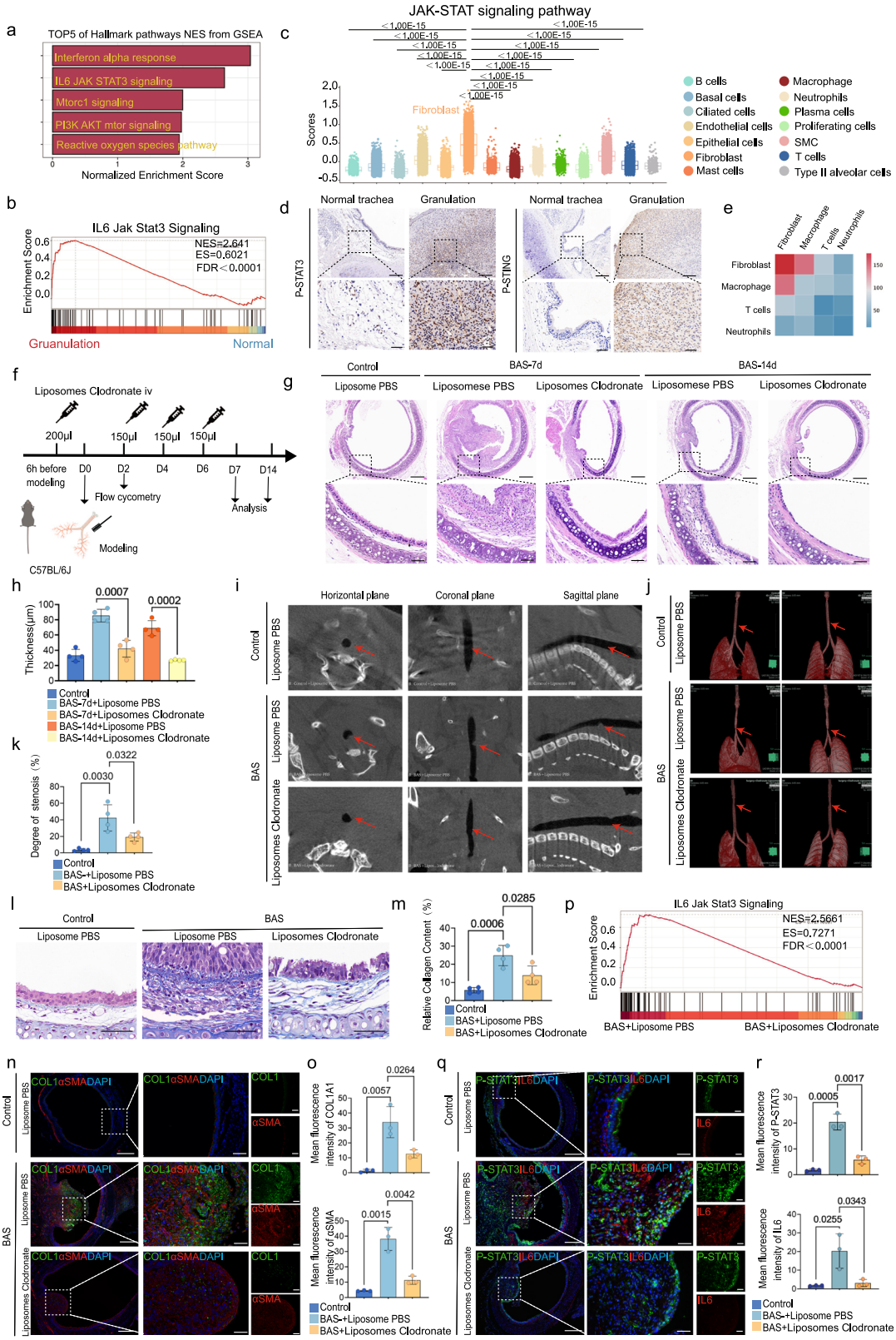

may play key roles in the pathogenesis of BAS by modulating the local immune environment and enhancing inflammatory responses. Therefore, targeting these cytokines may open new therapeutic avenues for treating BAS.

The role of the cGAS–STING pathway in fibrotic diseases is complex and multifaceted. While the present study focused on the profibrotic effects of STING activation in patients with benign airway stenosis (BAS), it is important to acknowledge the literature that presents contrasting findings. For example, certain studies have demonstrated that STING may exert antifibrotic effects in specific contexts, such as chronic pancreatitis and pulmonary fibrosis[43,44]. These opposing roles of STING may be influenced by various factors, including disease models, the type of tissue involved, the stage of disease progression, and the microenvironment. By addressing this complexity, the present study provides

Fig. 6 | Macrophages promote fibroblast activation via the IL6-STAT3 axis. **a** GSEA analysis showing TOP5 enriched hallmark pathways in Granulation group compared with Normal group. **b** GSEA analysis show IL6 jak STAT3 pathway enrichment in Granulation group. **c** Box Plot showing the JAK-STAT pathway score in all clusters in Normal group and Granulation group: B cells ($n = 1434$), basal cells(n = 10982), ciliated cells ($n = 1317$), endothelial cells ($n = 7241$), epithelial cells ($n = 5123$), fibroblasts ($n = 6808$), mast cells ($n = 475$), macrophages ($n = 5625$), neutrophils ($n = 10178$), plasma cells ($n = 1249$), proliferating cells ($n = 824$), SMCs ($n = 3608$), T cells ($n = 3500$) and Type II alveolar cells ($n = 222$). n represents the number of cells in cluster. **d** Representative images of P-STAT3 and P-STING immunohistochemical staining. ($n = 3$ sample per group). **e** Heatmap illustrates ligand-receptor interactions between Macrophages, T cells, neutrophils, and fibroblasts. **f**–**r** Mice were divided into three groups: control, BAS + PBS and BAS + Clodronate Liposomes. **f** Schematic of Clodronate Liposomes administration in mice. **g** Representative images of H&E staining in different groups at days 7 and 14. **h** Quantitative analysis of LP thickness in different groups. ($n = 4$ mice per group). **i** Micro CT scans of different groups in Horizontal, Coronal and Sagittal plane. **j** SYNPASE 3D reconstruction of mouse trachea. Red arrows indicating the stenosis site in (**i**–**k**). The CT diagram of the area of tracheal stenosis measured by SYNPASE 3D and quantitative analysis of area in different groups(n = 4 mice per group). **l** Representative images of Masson staining in different groups. **m** Quantitative analysis of collagen area in different groups ($n = 4$ mice per group). **n**, **o** Representative tracheal immunofluorescence images and mean fluorescence intensity of αSMA(red) and COL1(green) in different groups ($n = 3$ mice per group). **p** GSEA analysis show IL6 jak STAT3 pathway enrichment in BAS + PBS group. **q**, **r** Representative tracheal immunofluorescence images and mean fluorescence intensity of P-STAT3(green) and IL6(red) in different groups ($n = 3$ mice per group). Scale bars in (**d**, **g**, **n**, **q**) indicates 200 μm and 50 μm. Scale bars in (**l**) indicate 50 μm. In (**c**), box bounds shows 25th and 75th percentiles, whiskers shows 25th percentiles minus 1.5*IQR to 75th percentiles plus 1.5*IQR and box center shows the median. Data are presented as the mean ± SEM. One-way ANOVA analysis followed by Tukey post hoc multi-comparison test was used in (**h**, **k**, **m**, **o**, **r**). One-way ANOVA analysis followed by Duncan multiple- range test was used in **c**. Source data are provided as a Source Data file.

a better understanding of the involvement of the STING pathway in fibrosis, ultimately guiding further investigations into its therapeutic potential across different fibrotic diseases.

In conclusion, the present findings indicated that the cGAS–STING pathway plays a critical role in BAS through mainly promoting the release of the IL6 inflammatory factor from macrophages to activate STAT3 in fibroblasts, thereby promoting fibrosis. Therefore, the cGAS–STING pathway may represent a therapeutic target for preventing BAS.

Methods

Animals

C57BL/6 J, female and male mice, 8 weeks of age, were purchased from SPF (Beijing) Biotechnology Co., Ltd. The *STING* KO mice (Cat No. T012747), 8 weeks of age, were C57BL/6 J background, and were purchased from Jiangsu Gempharmatech, China. All animal were fed in Specific pathogen free (SPF) class animal houses at the First Hospital of the Naval Medical University with a standard 12 h light/12 h dark conditions and had free access to water and food. The room temperature was maintained at 20 ~ 26 °C, and relative humidity was around 40% ~ 70%. All animal experiments were performed in accordance with the Guide for the Care and Use of Laboratory Animals published by the NIH and approved by the Animal Care and Utilization Committee of Shanghai Changhai Hospital under number CHEC2021-006.

The incidence of benign airway stenosis does not differ between males and females[45]. In this study, we used both male and female mice and found that the severity of benign airway stenosis also did not differ between the two groups.

Patients and samples

All procedures performed in the study were approved by the Ethical Committee of The First Affiliated Hospital of Naval Medical University. The study was performed after obtaining written informed consent from the patients following the principles outlined in the Declaration of Helsinki. The ethical approval number was CHEC2021-043. The information of participants was summarized in Supplementary Table 1.

A total of seven samples were obtained for single-cell RNA sequencing. In the granulation group, 4 samples of granulation tissue from patients with benign airway stenosis were collected by Bronchoscopic Electrosurgical Snaring at The First Affiliated Hospital of Naval Medical University (ShangHai, China). The selection criterion of granulation tissue was the newly formed granulation tissue within one month of recent tracheal injury. In the normal group, 3 samples of normal trachea from patients undergoing lobectomy at The First Affiliated Hospital of Naval Medical University (ShangHai, China). The normal trachea was obtained by separating the lung tissue after lobectomy.

A total of ten tracheal lavage fluids were used to detect the content of dsDNA. In the BAS group ($n = 5$), the area of the injured trachea in patients with tracheal intubation was irrigated by tracheoscopy at The First Affiliated Hospital of Naval Medical University (ShangHai, China), and tracheal lavage fluid was collected. In the control group ($n = 5$), tracheal lavage fluid was obtained from patients with pulmonary nodules who underwent bronchoscopy at The First Affiliated Hospital of Naval Medical University (ShangHai, China) and whose airways had not been damaged.

A total of six samples were obtained for Immunohistochemistry.3 samples in control group and 3 samples in BAS group. These samples were obtained in the same way as those obtained for single-cell RNA sequencing.

Drug administration

For deplete macrophages in mice, the mice were given 200 μl of Clodronate Liposomes (#40337ES10, YEASEN, Shanghai, China) by intravenous Injection on 6 h before surgery and 150 μl of Clodronate Liposomes by intravenous Injection on days 2, 4 and 6 after surgery. The efficiency of macrophages depletion was evaluated by Flow Cytometry.

For inhibit STING in mice, the mice were given 5 mg/kg C176(#S6575, Selleck, USA) dissolved in 10% DMSO (# HY-Y0320, Med-Chem Express, USA) and 90% corn oil(#HY-Y1888, Med-Chem Express, USA) by intraperitoneal injection on 2 h before modeling, days 2, 4 and 6 after modeling.

For inhibit P-STAT3 in mice, the mice were given 10 mg/kg Stattic(#HY-13818, Med-Chem Express, USA) dissolved in 10% DMSO + 40% PEG300(#HY-Y0873, Med-Chem Express, USA) + 5%Tween-80(#HY-Y1891, Med-Chem Express, USA) + 45% saline by intraperitoneal injection on 2 h before modeling, days 2, 4 and 6 after modeling.

For inhibit cGAS in mice, the mice were given 5 mg/kg RU.521(#HY-114180, Med-Chem Express, USA) dissolved in 10% DMSO + 40% PEG300 + 5% Tween-80 + 45% saline by intraperitoneal injection on 2 h before modeling, days 2, 4 and 6 after modeling.

To investigate the role of IL6, Anti-mouse IL6-InVivo MP5–20F3 (#A2118, Selleck, USA) and recombinant mouse IL6(#HY-P7063, Med-Chem Express, USA) were used. For experiments utilizing Anti-mouse IL6-InVivo MP5–20F3 (8 mg/kg) was intraperitoneal injection on 2 h before modeling, days 2, 4 and 6 after modeling. For experiments utilizing recombinant mouse IL6(400 ng/mouse) was intravenous Injection on 2 h before modeling, days 2, 4 and 6 after modeling.

For DNase I treatment, Mice were treated with extracellular DNase I (200 μg/mouse) (#10104159001,Sigma-Aldrich,USA) 4 h prior and 8 h after modeling[13].

Transfection of siRNA

siRNAs were purchased from HANBIO(ShangHai,China). A scrambled siRNA was used as an NC. The target sequences of the siRNAs and siNC are presented in Supplementary Table 2. Transfections were

https://doi.org/10.1038/s41467-024-55170-5

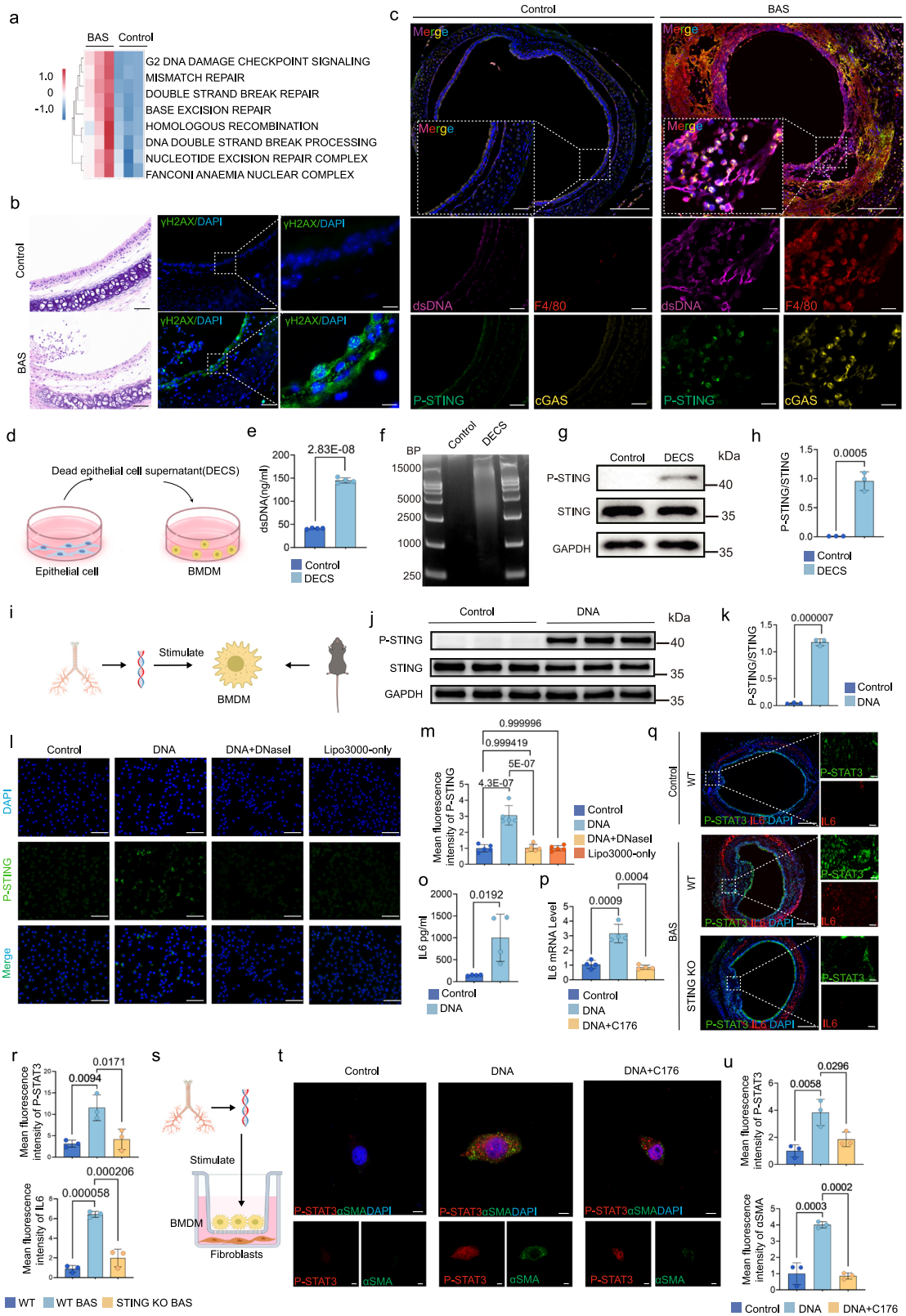

conducted with Lipo3000. SiRNAs were transfected at a final concentration of 50 nM, and subsequent experiments were performed 48 h after transfection.

Cell culture and treatment

Femur and tibia bones were harvested from C57BL/6 J mice, and bone marrow was flushed with PBS, centrifuged, and resuspended in Lysing Buffer (#555899, BD Pharmingen) to lyse red blood cells for 1 min. Then, blocked with RPMI-1640 medium (10% FBS) and centrifuged. Pellet was resuspended and cultured in RPMI-1640 medium (10% FBS, 1% penicillin, and streptomycin) and 25 ng/mL M-CSF (HY-P7085, MedChem Express, USA) for 7days to induce differentiation to BMDMs.

The mouse tracheal DNA were extracted by Tissue DNA Isolation Mini Kit (DC102, Vazyme, CHINA) and then BMDMs stimulated

Fig. 7 | dsDNA activates the STING pathway in macrophages thereby promoting fibroblast activation via the IL6-STAT3 axis. a Gene ontology (GO) functional enrichment analysis showed that the enriched DNA damage and repair genes in the BAS group at 24 h after tracheal injury compare to control group ($n = 3$ mice per group). **b** Representative images of H&E staining and immunofluorescence of γH2AX(green) in mouse trachea($n = 3$ mice per group). Scale bars indicate 50 μm in H&E staining images, 50 μm and 10 μm in immunofluorescence images. **c** Representative tracheal immunofluorescence images of dsDNA(pink), F4/80(red), P-STING (green), cGAS(yellow) in mouse trachea ($n = 3$ mice per group). Scale bars indicate 200 μm and 50 μm. **d** Schematic of use DECS to stimulate BMDMs. **e** Quantification analysis of dsDNA in cell culture supernatant in control group and DECS group ($n = 4$ independent experiments). **f** Representative images of AGAR gel electrophoresis of cell supernatants from control and DECS groups ($n = 3$ independent experiments). **g**, **h** Protein levels of phosphorylated STING in BMDM group stimulated with or without DECS, $n = 3$ independent experiments. **i** Schematic of BMDMs from WT mice stimulated by transfection of mouse tracheal DNA by lipo3000. **j**, **k** Protein levels of phosphorylated STING in the BMDM group stimulated with or without DNA ($n = 3$ independent experiments). **l** Representative immunofluorescence images of P-STING(green) in BMDM, Scale bars indicate 50 μm. **m** Quantitative analysis of relative Mean fluorescence intensity of P-STING ($n = 5$ independent experiments). **o** Protein levels of IL6 in the supernatant of BMDM group stimulated with or without DNA ($n = 4$ independent experiments). **p** mRNA levels of *IL6* in control group, DNA stimulated group and DNA stimulated group treated with C176 ($n = 4$ independent experiments). **q**, **r** Representative tracheal immunofluorescence images of and quantitative analysis of mean fluorescence intensity of P-STAT3(green) and IL6(red) in the different groups ($n = 3$ mice per group). Scale bars indicate 200 μm and 20 μm. **s** Schematic diagram depicting in-vitro co-culture model. **t**, **u** Representative immunofluorescence images of and quantitative analysis of mean fluorescence intensity of P-STAT3(red) and αSMA(-green) in fibroblasts ($n = 3$ independent experiments). Scale bars indicate 10 μm. Data are presented as the mean ± SEM. A two-sided student's T-test was used in (**e**, **h**, **k**, **o**). One-way ANOVA analysis followed by Tukey post hoc multi-comparison test was used in (**m**, **p**, **r**, **u**). Source data are provided as a Source Data file.

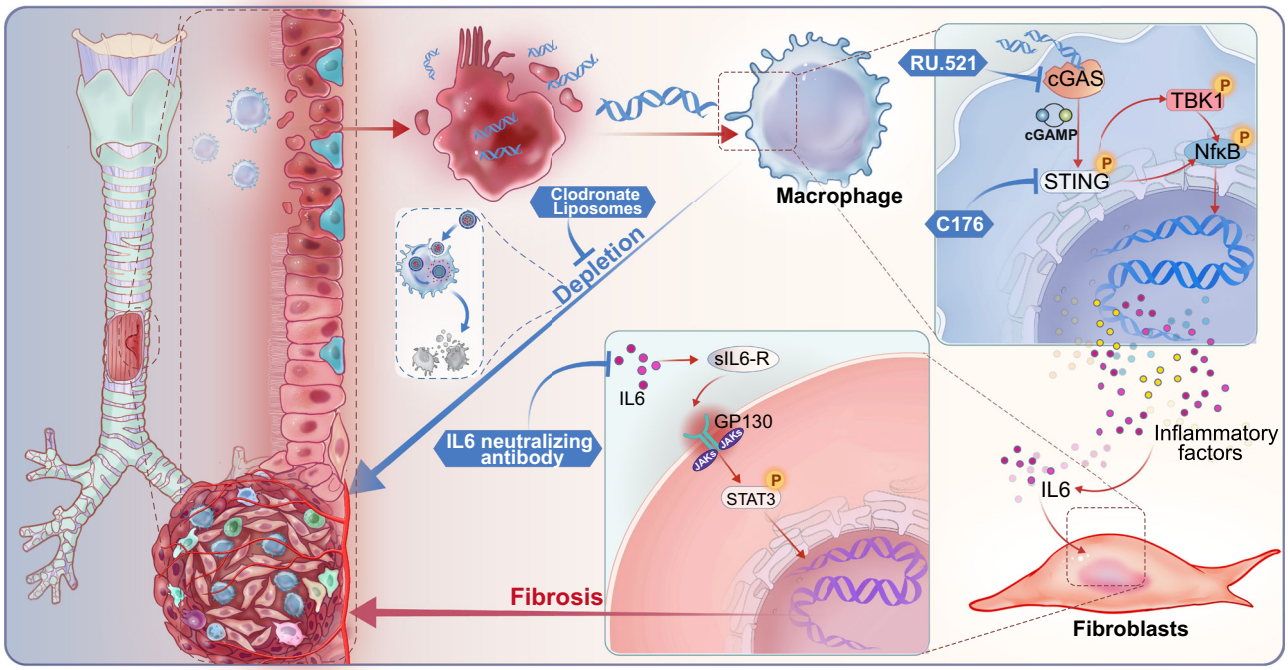

Fig. 8 | Schematic diagram of tracheal dsDNA activating cGAS-STING pathway of macrophages to promote fibrosis in BAS. Upon injury, dsDNA released from the tracheal epithelium activates the STING pathway in macrophages, leading to the release of the inflammatory cytokine IL-6. IL-6 then activates STAT3 signaling in fibroblasts, contributing to the fibrosis of granulation tissue. Treatment with the cGAS inhibitor RU.521, the STING inhibitor C176, or IL-6 neutralizing antibody alleviates granulation tissue fibrosis. Additionally, depletion of macrophages using bisphosphonate liposomes reduces the extent of fibrosis in the granulation tissue.

by transfection of mouse tracheal DNA by Lipofectamine3000(#L3000015, Thermo Fisher Scientific, USA). For DNase I Treatment, BMDMs culture medium were treated with 1 μg/mL DNase I 3 h prior, and 250 μg/ml DNase I after transfection reagents added[13,46].

Mouse lung epithelial cells MLE12 were purchased from ShangHai KuiSai BioTechnology Co Ltd (#QuiCell-M212). Epithelial cell death was induced by using UV light irradiation, and dead epithelial cells supernatants (DECS) were collected to culture BMDM for 24 h.

Mouse tracheal fibroblasts were purchased from Procell (#CP-M008). Fibroblasts were stimulated by transfection of tracheal DNA for active STING, and *STING* was knocked down in fibroblasts by transfection of siRNA. To explore the effect of inflammatory factors secreted by macrophages on fibroblasts, fibroblasts and BMDMs were cocultured in a Transwell culture system, the fibroblasts were seeded into the bottom of a 6-well plate while the BMDMs were seeded into the 6-well culture inserts. Prior to coculture, the BMDMs were treated with transfection mouse tracheal DNA. The pretreated BMDMs were then cocultured with fibroblasts.

All Cell lines were cultured in RPMI-1640 medium (Hyclone, USA) with 10% fetal bovine serum (#SH30406.05, Hyclone, USA), 1% penicillin and streptomycin(#SV30010,, Hyclone, USA) at 37 °C in a 5% CO_2 atmosphere.

Surgical procedure

Constructing a mouse model of benign airway stenosis by causing damage to the mouse trachea with a small brush (Supplementary

Fig. 11). For the procedure, the mouse was anesthetized by IP injection of a mixture of ketamin (100 mg/kg) and xylazine (10 mg/kg). Firstly, after sterilisation of the skin with 75% alcohol, a 1.5 cm incision was made in the anterior cervical skin of the mouse, and the trachea was fully exposed after bluntly separating the glands and the pre-tracheal muscles. Then, the trachea was incised transversely along the two tracheal cartilages below the cricoid cartilage, and with an incised length of two thirds of the circumference. Next a diameter of 1 mm small brush was inserted through cannula of safety IV catheter 20 G (B | BRAUN Medical) into the trachea 6 mm deep, then pull the cannula out of the trachea by pulling the line tied to cannula, leaving the brush in the trachea and scraping for three times to cause damage to the tracheal wall. Finally, the incised trachea was closed with 6-0 sutures and the subcutaneous tissue and skin were closed with 3-0 sutures. The mice were euthanized by cervical dislocation under 3% isoflurane anesthesia.

The control mice underwent sham surgery, in which the mice's trachea was cut, but the trachea was not injured with a small brush.

Measurement of dsDNA

Benign airway stenosis mice were collected for tracheal tissue 24 h after modelling. The interior of the trachea was then irrigated three times with 50 μl of TE buffer and the trachea lavage fluid was collected. Tracheal lavage fluid was collected in patients with BAS as well as in controls as described in Patiens and Samples. dsDNA was measured in the mouse trachea lavage fluid, human trachea lavage fluid and DECS using Picogreen dsDNA Quantitation Reagent (#12640ES60, YEASEN, Shanghai, China), according to the manufacturer's protocol.

Histology

The tracheas were fixed in 4% buffered formaldehyde for 24 h, paraffin-embedded, Slides were made from 3-μm-thick sections cut through in an axial plane, which were then stained with hematoxylin-eosin, Masson trichrome reagents. Masson-stained collagen area was measured by Image J software.

Tracheal Lamina Propria measurements

Measurements of the LP layer was performed as described in the literature[34,47]. To measure the thickness of the LP layer, the tracheal cartilage ring was divided into five segments, and the thickness of LP layer was measured from the medial side of the cartilage to the epithelial basement membrane. The thickest part of each segment was measured and recorded, and the mean LP layer thickness was calculated for each sample. A schematic of the measurement is shown in Supplementary Fig. 12.

Immunohistochemistry

For immunohistochemistry (IHC), the antigen was retrieved by incubation at 95 °C in citric acid antigen repair solution for 30 min, the slides were immunestained with anti-STING (D2P2F) from Rabbit (1:100, #13647, Cell Signaling Technology), anti-Phospho-Stat3 (Tyr705) (D3A7) from Rabbit (1:100, #9145, Cell Signaling Technology) and anti-Phospho-STING (Ser366) (E9A9K) from Rabbit (1:1600, #50907, Cell Signaling Technology) at 4 °C overnight. Binding antibodies were detected using biotinylated goat anti-rabbit secondary antibodies and incubated for 1 h at room temperature. The sections were then developed with DAB solution, and counterstained with hematoxylin.

Immunofluorescence staining of tracheal and cells

Tracheal tissues were fixed in 4% buffered formaldehyde for 24 h, embedded in paraffin, and sectioned at 3 μm. The tracheal tissues were incubated with primary antibodies overnight at 4 °C, followed by a 2 h incubation with the secondary antibody. Antibodies were used for immunofluorescence staining in the study: anti-STING (E9X7F) from Rabbit (1:400, #78827, Cell Signaling Technology), anti-Phospho-STING (Ser365) (D1C4T) from Rabbit (1:50, #62912, Cell Signaling Technology), anti-F4/80 (D4C8V) from Rabbit (1:400,#30325, Cell Signaling Technology), anti-Phospho-Stat3 (Tyr705) (D3A7) from Rabbit (1:200, #9145,Cell Signalling Technology), anti-cGAS from Rabbit (1:200, #29958-1-AP, Proteintech), anti-Collagen I(RM11310) from Rabbit (1:100,#ab316222,Abcam), anti-αSMA(D4K9N) from Rabbit(1:200,#19245,Cell Signaling Technology), anti-Phospho-Histone H2A.X (Ser139) (20E3) from Rabbit (1:200,#9718,Cell Signaling Technology), anti-IL-6 (D5W4V) from Rabbit (1:200,#12912, Cell Signaling Technology),dsDNA Marker from mice (1:100, #sc-58749, Santa Cruz Biotechnology).

Cells were fixed in 1% paraformaldehyde for 15 min, permeabilized with 0.3% Triton-X100/PBS, and blocked with 4% BSA. Cells were then incubated with in blocking buffer. Subsequently, the coverslips were incubated with secondary antibodies for 1 h at room temperature and finally stained with DAPI for 5 min at room temperature. Antibodies were used for immunofluorescence staining in the study: anti-Phospho-STING (Ser365) (D1C4T) from Rabbit (1:400, #62912, Cell Signaling Technology), anti-Phospho-Stat3 (Tyr705) (D3A7) from Rabbit (1:100, #9145, Cell Signaling Technology), anti-αSMA(D4K9N) from Rabbit (1:200, #19245, Cell Signaling Technology)

qRT-PCR

To obtain mRNA, we use a RNeasy extraction kit (#RC112, Vazyme, Nanjing, China) to extract mRNA from tracheal tissues and intracellular components. cDNA was generated with a One-step iScript cDNA Synthesis Kit (#R323, Vazyme, Nanjing, China), and qRT-PCR was performed using SYBR green Master Mix (#Q711, Vazyme, Nanjing, China) on QuantStudio 3 System (Thermo Fisher Scientific). The *GAPDH* gene was used as the control Data were analyzed using the comparative analysis of relative expression by $2^{-\Delta\Delta Ct}$ methods. The primers used in this study are listed in Supplementary Table 3.

Western blotting

Mouse tracheal tissues and cellular proteins were extracted using a lysis buffer prepared by proportionally mixing RIPA buffer, protease inhibitor, and phosphatase inhibitor. Protein concentration was determined using the BCA method, and samples were mixed with loading buffer and boiled at 100 °C for 10 min. A polyacrylamide gel with sodium dodecyl sulfate (SDS) was prepared. Then equal amounts of protein samples and Protein Ladder (#WJ103, Epizyme) were loaded into the wells for electrophoresis (at 80–120 V for 60 min). A methanol-based transfer buffer was prepared, and proteins were transferred onto a 0.45 μm PVDF membrane, followed by blocking in a blocking solution. The membrane was incubated overnight at 4 °C with primary antibodies, including anti-STING (D2P2F) from Rabbit (1:1000, #13647, Cell Signaling Technology), anti-Phospho-STING (Ser365) (D8F4W) from Rabbit (1:1000, #72971, Cell Signaling Technology), anti-TBK1(E8I3G) from Rabbit (1:1000, #38066, Cell Signaling Technology), anti-Phospho-TBK1(Ser172) (D52C2) from Rabbit (1:1000, #5483, Cell Signaling Technology), anti-NF-κB p65 (D14E12) from Rabbit (1:1000, #8242, Cell Signaling Technology), anti-Phospho-NF-κB p65 (Ser536) (93H1) from Rabbit (1:1000, #3033, Cell Signaling Technology),anti-αSMA(D4K9N) from Rabbit (1:1000, #19245, Cell Signaling Technology), anti-Collagen I(RM11310) from Rabbit (1:1000, #ab316222, Abcam), anti-cGAS (D3O8O) from Rabbit (1:1000, #31659, Cell Signaling Technology),anti-AIM2 from Rabbit (1:1000, #63660S, Cell Signalling Technology) and anti-GAPDH from Rabbit (1:5000, #10494-1-AP, Proteintech).Next, the membrane was incubated with HRP-conjugated Goat anti-rabbit IgG (1:8000, #SA00001-2, Proteintech). After scanning the membrane with Tanon 5200 chemiluminescent imaging system (Shang Hai), protein bands were analyzed using ImageJ software.

Micro CT and measurement method of tracheal stenosis in imaging

On the seventh day post-modeling, the mouse airways were examined by microCT (90 kV, 0.065 mA, PINGSENG Healthcare) scanning, and the tracheal area was measured within the adipose window. The degree of narrowing at the most constricted level was measured using the following formula: (1 - s/S) * 100%, where s represents the area of the most constricted level of the trachea and S represents the average of the areas at the normal levels 3 mm above and below the most constricted level. SYNPASE 3D (SYNAPSE 3D V4.4, Fujifilm Medical, Tokyo, Japan) was utilized for measuring the mouse tracheal area and performing 3D reconstruction of the trachea.

Evaluation of lung function

The lung function data of mice was recorded by putting them into a WBP respiratory whole-body plethysmography (WBP-4MR, TOW, China). Benign airway stenosis (BAS) occurs primarily in the upper airways. Clinically, patients with upper airway narrowing often experience prolonged inspiratory time. So, inspiratory time (Ti) was chossed as the indicators adopted to assess lung function. Each mouse was tested for 30 min. The first 10 min were used to acclimate to the environment, and the average inspiratory time was calculated as the average of the inspiratory time of the last 20 min.

Flow cytometry

Mouse tracheal tissue was dissociated and cleaned with PBS, placed in dissociation enzyme solution (Liberase 100 ug/ml, Roche 5401119001, DNase I 40 ug/ml, Sigma 10104159001) in DMEM at 37 °C for 45 min, Then cut the undissociated tissue and continue to bathe at 37 for 60 min, After the dissociation, wash with 10 ml pre-cooled PBS, filter with 70um screen, centrifuge 500 g for 5 min.After centrifugation, the supernatant was poured away and cell precipitates were collected[48]. Then, perform cell staining using LIVE/DEAD Stain (#564406, BV510, BD Biosciences) and cell surface marker antibodies. After surface staining, fix and permeabilize using the BD Fixation/Permeabilization Kit (#554714, BD Pharmingen), followed by intracellular cytokine staining. Finally, it was detected by CytoFlexS (Beckman Coulter). Cells were stained with antibody to the following markers: Anti-CD45 from Rat (1:200, #557659, APC-CY7, BD Biosciences), anti-CD11b from Rat (1:200, #552850, PE-CY7, BD Biosciences), anti-F4/80 from Rat (1:200, #565411, BV421, BD Biosciences), anti-STING (E9X7F) from Rabbit (1:1600, #78827S, AF488, Cell Signaling Technology).

Inflammatory factor analysis

After tracheal tissue isolation, Luminex multiplex cytokine assays (#12009159, BIO-RAD, Hercules, CA, USA) were used to detect inflammatory cytokines ($n = 6$/control group, $n = 10$/BAS group) and were performed by LabEx (Shanghai, China) using the Luminex X-200, according to the manufacturer's protocol (Luminex, Austin, TX, USA). The Luminex multiplex cytokine assays could detect following Inflammatory factors and chemokines: IL6, CCL20, IL-1beta, CXCL5, TNF-alpha, GM-CSF, CX3CL1, CCL1, CXCL13, IL-16, IFN-gamma, CXCL10, IL-2, CXCL11, IL-4, CCL7, CCL12, CCL2, CCL22, CCL5, IL-10, CXCL1, CCL27, CCL17, CCL19, CXCL16, CXCL12, CCL24, CCL11, CCL4, CCL3.

Enzyme-linked immunosorbent assay was performed for the measurement of IL6(EK206, LIANKE) in cell culture supernatant according to the manufacturer's instructions.

AGAR gel electrophoresis

The detection samples were run in 1% agarose gels, cast from molecular biology grade agarose (#RM02852,Abclone,WuHan,China) dissolved in 1×TBE buffer. The cell supernatant was mixed with DNA loading buffer (#RK30151, Abclone, WuHan, China) and added to the lane for electrophoresis with DNA marker (#RK30192, Abclone, WuHan, China), which was run at 90 V at room temperature for 25 min. Imaging was completed on Tanon 3500B (Shang Hai) automatic gel image analysis system.

Bulk RNA extraction library construction and sequencing

We performed bulk RNA sequencing twice in total. The first was to detect genetic differences in mice with BAS at different time points (Control=3 mice, BAS-24h = 3 mice and BAS-7d = 3 mice), and the second was to investigate the effect of macrophage depletion on BAS (Control=3 mice, BAS-7d = 3 mice and BAS-7 d with Clodronate Liposomes =3 mice).

Mouse tracheal tissues were collected, and each trachea was an independent sample. Total RNA was extracted using Trizol reagent (thermofisher, 15596018) following the manufacturer's procedure. The total RNA quantity and purity were analysis of Bioanalyzer 2100 and RNA 6000 Nano LabChip Kit (Agilent, CA, USA, 5067-1511), high-quality RNA samples with RIN number > 7.0 were used to construct sequencing library. After total RNA was extracted, mRNA was purified from total RNA (5ug) using Dynabeads Oligo (dT) (Thermo Fisher, CA, USA) with two rounds of purification. Following purification, the mRNA was fragmented into short fragments using divalent cations under elevated temperature (Magnesium RNA Fragmentation Module (NEB, cat.e6150, USA) under 94 °C 5–7 min). Then the cleaved RNA fragments were reverse-transcribed to create the cDNA by SuperScript II Reverse Transcriptase (Invitrogen, cat. 1896649, USA), which were next used to synthesise U-labeled second-stranded DNAs with E. coli DNA polymerase I (NEB, cat.m0209, USA), RNase H (NEB, cat.m0297, USA) and dUTP Solution (Thermo Fisher, cat.R0133, USA). An A-base was then added to the blunt ends of each strand, preparing them for ligation to the indexed adapters. Each adapter contained a T-base overhang for ligating the adapter to the A-tailed fragmented DNA. Dual-index adapters were ligated to the fragments, and size selection was performed with AMPureXP beads. After the heat-labile UDG enzyme (NEB, cat.m0280, USA) treatment of the U-labeled second-stranded DNAs, the ligated products were amplified with PCR. The average insert size for the final cDNA librarys were 300 ± 50 bp. At last, we performed the 2 × 150 bp paired-end sequencing (PE150) on an Illumina Novaseq 6000 (LC-Bio Technology CO., Ltd., Hangzhou, China) following the vendor's recommended protocol.

Bulk-RNA sequencing analysis

A cDNA library constructed by technology from the pooled RNA from trachea of mice was sequenced run with Illumina Novaseq 6000 sequence platform. Using the Illumina paired-end RNA-seq approach, we sequenced the transcriptome, generating a total of millon 2 × 150 bp paired-end reads. Reads obtained from the sequencing machines includes raw reads containing adapters or low-quality bases which will affect the following assembly and analysis. Thus, to get high quality clean reads, reads were further filtered by Cutadapt (https://cutadapt.readthedocs.io/en/stable/, version: cutadapt-1.9). The parameters were as follows: 1) removing reads containing adapters; 2) removing reads containing polyA and polyG;3) removing reads containing more than 5% of unknown nucleotides (N);4) removing low quality reads containing more than 20% of low quality (Q-value ≤ 20) bases.

Then sequence quality was verified using FastQC (http://www.bioinformatics.babraham.ac.uk/projects/fastqc/, 0.11.9). including the Q20, Q30 and GC-content of the clean data. After that, a total of G bp of cleaned, paired-end reads were produced. We aligned reads of all samples to the mice reference genome using HISAT2 (https://daehwankimlab.github.io/hisat2/, version: hisat2-2.2.1) package, which initially remove a portion of the reads based on quality information accompanying each read and then maps the reads to the reference genome. Genes differential expression analysis was performed by DESeq2 software between two different groups (and by

edgeR between two samples). The genes with the parameter of false discovery rate (FDR) below 0.05 and absolute fold change ≥1 were considered differentially expressed genes.

The GO and KEGG enrichment analysis of differential genes can explain the functional enrichment of differential genes and clarify the differences between samples at the gene function level. We use cluster Profiler (v4.1.3) R software package for GO function enrichment and KEGG pathway enrichment analysis. When $P < 0.05$, it is considered that the GO or KEGG function is significantly enriched. Gene Set Enrichment Analysis (GSEA) was using software GSEA (v4.1.0) with the MSigDB (v7.5.1). Mufzz Analysis was using Fuzzy C-means Clustering algorithm (FCM) with Mufzz package (v 2.54.0) in R (v4.1.3).

All Bulk-RNA sequencing data analysis was performed using the OmicStudio tools created by LC-BIO Co., Ltd (HangZhou, China) at https://www.omicstudio.cn/cell.

Single-cell library preparation and sequencing

Sample collection methods are described in Patients and Samples. The tissue was cut into small pieces of 0.5 mm^2 and then washed with 1xPBS to dissociate the tissue into individual cells in dissociation solution. Overall cell viability exceeded 85%, as confirmed by trypan blue exclusion. Tissues were dissociated into single cells in dissociation solution (0.35% collagenase IV5,2 mg/ml papain, 120 Units/ml DNase I) in 37 °C water bath with shaking for 20 min at 100 rpm. Digestion was terminated with 1× PBS containing 10% fetal bovine serum (FBS, V/V) then pipetting 5–10 times with a Pasteur pipette。The resulting cell suspension was filtered by passing through 70–30 um stacked cell strainer and centrifuged at 300 g for 5 min at 4 °C. The cell pellet was resuspended in 100 ul 1× PBS (0.04% BSA) and added with 1 ml 1× red blood cell lysis buffer (MACS 130-094-183, 10×) and incubated at room temperature or on ice for 2–10 min to lyse remaining red blood cells. After incubation, the suspension was centrifuged at 300 g for 5 min at room temperature. The suspension was resuspended in 100 µl Dead Cell Removal MicroBeads(MACS 130-090-101) and remove dead cells using Miltenyi Dead Cell Removal Kit (MACS 130-090-101). Then the suspension was resuspended in 1× PBS(0.04% BSA) and centrifuged at 300 g for 3 min at 4 °C(repeat twice). The cell pellet was resuspended in 50 µl of 1× PBS (0.04% BSA). The overall cell viability was confirmed by trypan blue exclusion, which needed to be above 85%, single cell suspensions were counted using a haemocytometer/ Countess II Automated Cell Counter and concentration adjusted to 700–1200 cells/µl.

Single-cell suspensions were loaded to 10x Chromium to capture single cell according to the manufacturer's instructions of 10X Genomics Chromium Single-Cell 3' kit (V3). The following cDNA amplification and library construction steps were performed according to the standard protocol. Libraries were sequenced on an Illumina NovaSeq 6000 sequencing system (paired-end multiplexing run,150 bp) by LC-Bio Technology co.ltd., (HangZhou, China) at a minimum depth of 20,000 reads per cell.

Single-cell data analysis

Sequencing results were demultiplexed and converted to FASTQ format using Illumina bcl2fastq software(version2.20). Sample demultiplexing, barcode processing and single-cell 3'gene counting by using the Cell Ranger pipeline(https://support.10xgenomics.com/single-cell-geneexpression/ software/pipelines/latest/what-is-cell-ranger,version 3.1.0) and scRNA-seq data were aligned to Ensembl v110 homo_sapiens reference genome, a total of 67,390 single cell captured from 3 Normal group and 4 Granulation group were processed using 10X Genomics Chromium Single Cell 3'Solution.

The Cell Ranger output was loaded into Seurat (version 3.1.1) be used to Dimensional reduction, clustering, and analysis of scRNA-seq data. Overall 58,586 cells passed the quality control threshold: all genes expressed in less than three cells(default parameters:1 cell)were removed, number of genes expressed per cell å 100 as low and inf as high cut-off, NUMI had no limits, the percent of mitochondrial-DNA derived gene-expression < 25%.

To visualize the data, we further reduced the dimensionality of all 18,339 cells using Seurat and used UMAP to project the cells into 2D space. The steps include:1 Using the LogNormalize method of the "Normalization" function of the Seurat software to calculated the expression value of genes; 2 PCA (Principal component analysis) analysis was performed using the normalized expression value, within all the PCs, the top 10 PCs were used to do clustering and UMAP analysis;3 To find clusters, selecting weighted Shared Nearest Neighbor (SNN) graph-based clustering method. Marker genes for each cluster were identified with the Wilcoxon rank-sum test with default parameters via the FindAllMarkers function in Seurat. This selects markers genes which are expressed in more than 10% of the cells in a cluster and average log (Fold Change) of greater than 0.25.

For macrophage reclustering, macrophage clusters were subset and unsupervised clustering was used to identify macrophage subpopulations. Macrophage subsets were analyzed with FindMarkers, to characterize cluster identities and DGE between treatment conditions.

To investigate the potential functions, cluster Profiler (v4.1.32) R software package was used for Gene Ontology (GO) analysis, and software GSEA (v4.1.0) with the MSigDB (v7.5.1) were used for Gene Set Enrichment analysis (GSEA). Pathways with p value less than 0.05 were considered as significantly enriched. The cGAS-STING pathway scoring was based on the Addmodulescore function in Seurat (v 4.1.0). CellChat cell-cell interaction network analysis was used to characterize Immune cell-fibroblast interactions by Cellphonedb (v5.0.0).

All SingleCell Data Analysis was performed using the OmicStudio tools created by LC-BIO Co., Ltd (HangZhou, China) at https://www.omicstudio.cn/cell.

Statistical analysis

All dates are presented as mean ± SEM. GraphPad Prism 9 was used for statistical analysis (GraphPad software, San Diego, California, USA). Differences between two groups were identified using the two-sided Student's test and two-sided Mann Whitney test. Multiple groups using One-or two- way ANOVA analysis followed by Kruskal-Wallis's test and Duncan multiple- range test. Spearman correlation analysis was used to analyze the correlation between the two groups. P values of less than 0.05 were considered statistically significant.

Reporting summary

Further information on research design is available in the Nature Portfolio Reporting Summary linked to this article.

Data availability

All data supporting the findings of this study are available within the article and its supplementary files. Any additional requests for information can be directed to, and will be fulfilled by, the corresponding authors. Sequence raw data are available in the NCBI–SRA (Sequence Read Archive): Single Cell Sequencing (SRR31229501, SRR31229502, SRR31229503, SRR31229504, SRR31229505, SRR31229506, SRR31229507), Bulk RNA sequencing of benign airway stenosis mice (SRR30898181, SRR30898182, SRR30898183, SRR30898184, SRR30898185, SRR30898186, SRR30898187, SRR30898188, SRR30898189), Bulk RNA sequencing used to analyze the effect of macrophage depletion on BAS (SRR30831591, SRR30831592, SRR30831593, SRR30831594, SRR30831595, SRR30831596, SRR30831597, SRR30831598, SRR30831599). All other data are available in the article and its Supplementary files or from the corresponding author upon request. Source data are provided with this paper.

References

1. Oberg, C. L., Holden, V. K. & Channick, C. L. Benign Central Airway Obstruction. *Semin Respir. Crit. Care Med.* **39**, 731–746 (2018).
2. Piazza, C. et al. Long-term intubation and high rate of tracheostomy in COVID-19 patients might determine an unprecedented increase of airway stenoses: a call to action from the European Laryngological Society. *Eur. Arch. Otorhinolaryngol.* **278**, 1–7 (2021).
3. Guibert, N., Saka, H. & Dutau, H. Airway stenting: Technological advancements and its role in interventional pulmonology. *Respirology* **25**, 953–962 (2020).
4. Sun, K. et al. Long-term prognostic factors of clinical success after interventional bronchoscopy in patients with scarring central airway stenosis. *BMC Pulm. Med.* **21**, 73 (2021).
5. Chen, N. et al. Inhibitory effect of mitomycin C on proliferation of primary cultured fibroblasts from human airway granulation tissues. *Respiration* **85**, 500–504 (2013).
6. Li, X. et al. Treatment of scarring central airway stenosis with pirfenidone: Case report. *Med. (Baltim.)* **101**, e31354 (2022).
7. Qiu, X. et al. Paclitaxel-Loaded PLGA Coating Stents in the Treatment of Benign Cicatrical Airway Stenosis. *J. Clin. Med* **11**, 517 (2022).
8. Enyuan, Q. et al. Erythromycin combined with corticosteroid reduced inflammation and modified trauma-induced tracheal stenosis in a rabbit model. *Ther. Adv. Respir. Dis.* **12**, 1753466618773707 (2018).
9. Huang, Z. et al. Protective effects of different anti-inflammatory drugs on tracheal stenosis following injury and potential mechanisms. *Mol. Med Rep.* **23**, 314 (2021).
10. Konno, H. & Barber, G. N. The STING controlled cytosolic-DNA activated innate immune pathway and microbial disease. *Microbes Infect.* **16**, 998–1001 (2014).
11. Chen, Q., Sun, L. & Chen, Z. J. Regulation and function of the cGAS-STING pathway of cytosolic DNA sensing. *Nat. Immunol.* **17**, 1142–1149 (2016).
12. Barber, G. N. STING: infection, inflammation and cancer. *Nat. Rev. Immunol.* **15**, 760–770 (2015).
13. Benmerzoug, S. et al. STING-dependent sensing of self-DNA drives silica-induced lung inflammation. *Nat. Commun.* **9**, 5226 (2018).
14. Wang, X. et al. STING expression in monocyte-derived macrophages is associated with the progression of liver inflammation and fibrosis in patients with nonalcoholic fatty liver disease. *Lab Invest* **100**, 542–552 (2020).
15. Zeng, H. M. et al. Pharmacological Inhibition of STING/TBK1 Signaling Attenuates Myeloid Fibroblast Activation and Macrophage to Myofibroblast Transition in Renal Fibrosis. *Front. Pharmacol.* **13**, https://doi.org/10.3389/fphar.2022.940716 (2022).
16. Kessler, N. et al. Monocyte-derived macrophages aggravate pulmonary vasculitis via cGAS/STING/IFN-mediated nucleic acid sensing. *J. Exp. Med.* **219**. e20220759 (2022).
17. Minutti, C. M. et al. Tissue-specific contribution of macrophages to wound healing. *Semin Cell Dev. Biol.* **61**, 3–11 (2017).
18. Hu, S. et al. The selective STING inhibitor H-151 preserves myocardial function and ameliorates cardiac fibrosis in murine myocardial infarction. *Int Immunopharmacol.* **107**, 108658 (2022).
19. Dvorkin, S. et al. New frontiers in the cGAS-STING intracellular DNA-sensing pathway. *Immunity* **57**, 718–730 (2024).
20. Zhang, Z. et al. Multifaceted functions of STING in human health and disease: from molecular mechanism to targeted strategy. *Signal Transduct. Target Ther.* **7**, 394 (2022).
21. Zou, M. et al. Inhibition of cGAS-STING by JQ1 alleviates oxidative stress-induced retina inflammation and degeneration. *Cell Death Differ.* **29**, 1816–1833 (2022).
22. Hu, B. et al. The DNA-sensing AIM2 inflammasome controls radiation-induced cell death and tissue injury. *Science* **354**, 765–768 (2016).
23. Wan, D., Jiang, W. & Hao, J. Research Advances in How the cGAS-STING Pathway Controls the Cellular Inflammatory Response. *Front Immunol.* **11**, 615 (2020).
24. Zhang, C. et al. Intercellular mitochondrial component transfer triggers ischemic cardiac fibrosis. *Sci. Bull. (Beijing)* **68**, 1784–1799 (2023).
25. Liu, C. et al. DNA from macrophages induces fibrosis and vasculopathy through POLR3A/STING/type I interferon axis in systemic sclerosis. *Rheumatol. (Oxf.)* **62**, 934–945 (2023).
26. Decout, A. et al. The cGAS-STING pathway as a therapeutic target in inflammatory diseases. *Nat. Rev. Immunol.* **21**, 548–569 (2021).
27. Hesketh, M. et al. Macrophage Phenotypes Regulate Scar Formation and Chronic Wound Healing. *Int J. Mol. Sci.* **18**, 1545 (2017).
28. Nam, S. & Lim, J. S. Essential role of interferon regulatory factor 4 (IRF4) in immune cell development. *Arch. Pharm. Res* **39**, 1548–1555 (2016).
29. Bharadwaj, U. et al. Targeting Janus Kinases and Signal Transducer and Activator of Transcription 3 to Treat Inflammation, Fibrosis, and Cancer: Rationale, Progress, and Caution. *Pharm. Rev.* **72**, 486–526 (2020).
30. Montero, P. et al. Role of JAK/STAT in Interstitial Lung Diseases; Molecular and Cellular Mechanisms. *Int. J. Mol. Sci.* **22**, https://doi.org/10.3390/ijms22126211 (2021).
31. Feng, T. M. et al. Involvement of PD-1(+)CD4(+) T cells in the development of traumatic tracheal stenosis by regulating the IL-17/STAT3 pathway. *Biochim Biophys. Acta Mol. Basis Dis.* **1870**, 167216 (2024).
32. Yu, Y. et al. Cytosolic DNA–Mediated STING-Dependent Inflammation Contributes to the Progression of Psoriasis. *J. Invest. Dermatol.* **142**, 898–906.e4 (2022).
33. Marchioni, A. et al. Molecular Mechanisms and Physiological Changes behind Benign Tracheal and Subglottic Stenosis in Adults. *Int J. Mol. Sci.* **23**, 2421 (2022).
34. Motz, K. M. et al. Sirolimus-eluting airway stent reduces profibrotic Th17 cells and inhibits laryngotracheal stenosis. *JCI Insight.* **8**. https://doi.org/10.1172/jci.insight.158456 (2023).
35. Gao, L. et al. STING/ACSL4 axis-dependent ferroptosis and inflammation promote hypertension-associated chronic kidney disease. *Mol. Ther.* **31**, 3084–3103 (2023).
36. Zhang, Y. et al. STING-Dependent Sensing of Self-DNA Driving Pyroptosis Contributes to Radiation-Induced Lung Injury. *Int J. Radiat. Oncol. Biol. Phys.* **117**, 928–941 (2023).
37. Li, M. et al. Macrophage Related Chronic Inflammation in Non-Healing Wounds. *Front Immunol.* **12**, 6817 (2021).
38. Ou, L. et al. Targeting STING-mediated pro-inflammatory and pro-fibrotic effects of alveolar macrophages and fibroblasts blunts silicosis caused by silica particles. *J. Hazard Mater.* **458**, 131907 (2023).
39. Plikus, M. V. et al. Fibroblasts: Origins, definitions, and functions in health and disease. *Cell* **184**, 3852–3872 (2021).
40. Lee, C. C. et al. An updated review of the immunological mechanisms of keloid scars. *Front. Immunol.* **14**, 1117630 (2023).
41. Borthwick, L. A. The IL-1 cytokine family and its role in inflammation and fibrosis in the lung. *Semin Immunopathol.* **38**, 517–534 (2016).
42. Ning, L. et al. Cytosolic DNA-STING-NLRP3 axis is involved in murine acute lung injury induced by lipopolysaccharide. *Clin. Transl. Med.* **10**, e228 (2020).
43. Zhao, Q. et al. STING signalling protects against chronic pancreatitis by modulating Th17 response. *Gut* **68**, 1827–1837 (2019).
44. Savigny, F. et al. Protective Role of the Nucleic Acid Sensor STING in Pulmonary Fibrosis. *Front Immunol.* **11**, 588799 (2020).
45. Li, M. et al. Risk Factors for Posttracheostomy Tracheal Stenosis. *Otolaryngol. Head. Neck Surg.* **159**, 698–704 (2018).
46. Wang, X. et al. DNA sensing via the cGAS/STING pathway activates the immunoproteasome and adaptive T-cell immunity. *Embo J.* **42**, e110597 (2023).

47. Hillel, A. T. et al. An in situ, in vivo murine model for the study of laryngotracheal stenosis. *JAMA Otolaryngol. Head. Neck Surg.* **140**, 961–966 (2014).
48. Hillel, A. T. et al. Dysregulated Macrophages Are Present in Bleomycin-Induced Murine Laryngotracheal Stenosis. *Otolaryngol. Head. Neck Surg.* **153**, 244–250 (2015).

Acknowledgements

We are grateful for bioinformatics support from Qin Xie and XiaoLi Meng (LC-Bio Technology co.,ltd.).This work was supported by the National Natural Science Foundation of China with Grants number 82270112(C.B.) and 82000102(H.S.). The Fig. 2c, k, Fig.4a, Fig.5b, Fig.6f, Fig. 7i, s, Supplementary Fig. 5a, Supplementary Fig. 9b, e and Supplementary Fig. 10a partly Created by MedPeer (medpeer.cn), and has been confirmed by publication and licensing rights.

Author contributions

Y.C., H.S., and C.B. designed the study. Y.C., C.Y., and Y.M. conducted experiments and analyzed data. D.S., X.L., S.T., Y.Z., C.X., and Y.D. collected human specimens and three-dimensional reconstructions of microCT images from mice. Y.C. wrote the manuscript. C.H., H.S. and C.B. organized and supervised the study.

Competing interests

The authors declare no competing interests.

Additional information

Supplementary information The online version contains supplementary material available at https://doi.org/10.1038/s41467-024-55170-5.

Correspondence and requests for materials should be addressed to ChaoFeng Han, Hui Shi or Chong Bai.

Peer review information *Nature Communications* thanks Lars Lunding, Silke Meiners, Nicolas Riteau and the other, anonymous, reviewer(s) for their contribution to the peer review of this work. A peer review file is available.